Synthesis, Characterization and Environmental Application of a Magnetic LDH-Based $CoO•CuFe_2O_4$ Nanocatalyst

Ayodeji Olugbenga Ifebajo

Submitted to the
Institute of Graduate Studies and Research
in partial fulfillment of the requirements for the degree of

Doctor of Philosophy
in
Chemistry

Eastern Mediterranean University
September 2019
Gazimağusa, North Cyprus

Approval of the Institute of Graduate Studies and Research

Prof. Dr. Ali Hakan Ulusoy
Acting Director

I certify that this thesis satisfies all the requirements as a thesis for the degree of Doctor of Philosophy in Chemistry.

Prof. Dr. İzzet Sakallı
Chair, Department of Chemistry

We certify that we have read this thesis and that in our opinion it is fully adequate in scope and quality as a thesis for the degree of Doctor of Philosophy in Chemistry.

Assoc. Prof. Dr. Akeem Oladipo
Co-Supervisor

Prof. Dr. Mustafa Gazi
Supervisor

Examining Committee

1. Prof. Dr. Mustafa Gazi
2. Prof. Dr. Oya S. Okay
3. Prof. Dr. Turgay Seçkin
4. Prof. Dr. Elvan Yılmaz
5. Assoc. Prof. Dr. Hayrettin Ozan Gülcan

ABSTRACT

Herein, we synthesized a multipurpose $CoO•CuFe_2O_4$ magnetic mixed metal oxide (MMO) nanocatalyst from its corresponding Layered double hydroxide (CoCuFe LDH) via a simple co-precipitation method. The resultant magnetic $CoO•CuFe_2O_4$ MMO was well characterized using SEM, VSM, FTIR, XRD and UV–vis DRS. Thereafter, the potential of the as-synthesized magnetic nanocatalyst, $CoO•CuFe_2O_4$ MMO to remove tetracycline (TET) via adsorption and degrade Eriochrome Black T (EBT) via a combination of adsorption and sunlight assisted photocatalysis was then explored. The influence of varying adsorption and photocatalytic operational parameters including; contact time, pH, pollutant initial concentration, dosage, scavengers, temperature, interfering counter ions on the removal and degradation efficiency was also investigated systematically. Finally, the equilibrium adsorption data obtained at 298 K were analyzed using four two-parameter adsorption isotherms.

The characteristics results demonstrated that the average pore diameter, surface area and pH point zero charge of the $CoO•CuFe_2O_4$ MMO was 5.8 nm, 348.5 m^2/g and 5.8 respectively with an optical band gap of 2.1 eV. Also, the saturation magnetization, M_s of the calcined mixed metal oxide (83.2 emu/g) were higher than that of the LDH precursor (61.3 emu/g). The FTIR spectra confirmed the presence of OH-stretching and intercalated anions in the structure of the Co•Fe LDH which disappeared on calcination. Thus, confirming the formation of the $CoO•CuFe_2O_4$ MMO.

Results obtained from the adsorption studies of both TET and EBT showed that the solution pH had a significant effect on the adsorption potential of the $CoO•CuFe_2O_4$ MMO. Equilibrium adsorption data was well simulated by the Langmuir isotherm with maximum adsorption capacity for TET and EBT was 175.4 and 51.8 mg/g at pH 6.0 and 2.0. Thermodynamic parameters, enthalpy $\Delta H° = 27.35$ KJ/mol and Gibbs free energy change, $\Delta G° = -2.60 – -5.14$ KJ/mol confirmed that the adsorptive removal of TET was thermodynamically feasible and endothermic.

Catalytic potential of $CoO•CuFe_2O_4$ MMO was also evaluated for the removal of EBT. Results obtained shows that the degradation of EBT dye was very rapid and depends on the dye solution pH, catalyst dosage and substrate concentration. Optimum dosage and pH for EBT degradation was 1.0 g/L at pH 2.0. After 60 min of sunlight irradiation, 98%, 93% and 86% degradation was observed for 10, 20 and 40 ppm initial EBT concentration respectively. The proposed mechanism revealed that the photogenerated holes (h^+) were the main reactive specie responsible for the degradation of EBT dye. After six consecutive recycling runs, the removal and degradation efficiency of the regenerated $CoO•CuFe_2O_4$ MMO was still very high at ~ 93% and 80% for TET and EBT.

Overall, the findings in this study confirmed that the $CoO•CuFe_2O_4$ MMO can act as a suitable adsorbent for removal of TET and also as adsorbent/photocatalyst in the degradation of EBT from aqueous solution.

Keywords: photocatalysis, mixed metal oxides, tetracycline, azo dye, Eriochrome black T, adsorption

ÖZ

Burada, basit bir birlikte çöktürme yöntemi kullanarak tabakalı çift hidroksit (CoCuFe LDH) yapısında çok amaçlı CoO•$CuFe_2O_4$ manyetik karışık metal oksit (MMO) nanokatalist sentezlenmiştir. Oluşan manyetik CoO•$CuFe_2O_4$ MMO yapısı SEM, VSM, FTIR, XRD, ve UV-vis DRS kullanılarak detaylı bir şekilde karakterize edilmiştir. Daha sonra, sentezlenmiş olan manyetik nanokatalist CoO•$CuFe_2O_4$ MMO ' nun adsorpsiyonu ile Tetrasiklin (TET) uzaklaştırma ve adsorpsiyona ek olarak güneş ışığı destekli fotokataliz kombinasyonu ile Eriochrome Black T (EBT) boyasını parçalama potansiyeli araştırılmıştır. Uzaklaştırma ve parçalama verimi üzerine etki yapan temas süresi, pH, kirletici maddenin başlangıç konsantrasyonu, dozaj, temizleyiciler, sıcaklık ve engelleyici karşı iyonları da içeren çeşitli adsorpsiyon ve fotokatalitik işlem parametrelerinin etkileri de sistematik olarak araştırılmıştır. Sonuç olarak, 298 K sıcaklıkta elde edilen denge halindeki adsorpsiyon verisi dört adet iki-parametreli adsorpsiyon izotermi kullanılarak analiz edilmiştir.

CoO•$CuFe_2O_4$ MMO ' nun karakteristik özellik sonuçları ortalama por çapı, yüzey alanı ve sıfır yüklü pH değerinin sırasıyla 5.8 nm, 348.5 m^2/g ve 5.8 olduğuna ek olarak optik bant aralığının 2.1 eV olduğunu da göstermiştir. Ayrıca, kalsine karışık metal oksitin doygunluk mıknatıslanması, M_s (83.2 emu/g) LDH öncü maddesinden (61.3 emu/g) daha yüksek olduğu bulunmuştur. FTIR spektrumları Co•Fe LDH yapısındaki OH-uzamasının ve araya giren anyonların oluşturduğu görüntülerin kalsinasyon sonucu ortadan kalktığını onaylamıştır. Böylece, CoO•$CuFe_2O_4$ MMO yapısının oluşumu onaylanmıştır.

TET ve EBT için yapılan adsorpsiyon çalışmalarından elde edilen sonuçlar solüsyonun pH değerinin $CoO•CuFe_2O_4$ MMO nun adsorpsiyon potansiyelinde önemli bir etkisi olduğunu göstermiştir. Denge halindeki emilim verisi Langmuir izotermi kullanılarak iyi bir şekilde simüle edilmiş olup TET ve EBT için maksimum adsorpsiyon kapasitesi sırasıyla pH 6.0 değerinde 175.4 mg/g ve pH 2.0 değerinde 51.8 mg/g olarak bulunmuştur. Termodinamik parametreler, entalpi $\Delta H° = 27.35$ KJ/mol ve Gibbs serbest enerji değişimi, $\Delta G° = -2.60 – -5.14$ KJ/mol TET in adsorpsiyon ile uzaklaştırılmasının endotermik ve termodinamik olarak mümkün olduğunu onaylamıştır.

$CoO•CuFe_2O_4$ MMO ’ nun katalitik potansiyeli EBT ’ nin uzaklaştırılması ile değerlendirilmiştir. Elde edilen sonuçlar EBT boyasının parçalanmasının çok hızlı olmasının yanı sıra boya solüsyonunun pH değeri, katalist miktarı ve substrat konsantrasyonuna bağlı olduğunu göstermiştir. EBT parçalanması için optimum dozaj 1.0 g/L ve pH 2.0 olarak bulunmuştur. Başlangıç konsantrasyonu 10, 20 ve 40 ppm olan EBT ’ nin 60 dakika boyunca güneş ışınına maruz kalmasından sonra oluşan parçalanma oranlarının sırasıyla 98%, %93 ve 86% olduğu gözlemlenmiştir. Önerilen mekanizma foto jenere boşlukların (h^+) EBT boyasının parçalanmasındaki ana reaktif tür olduğunu ortaya çıkarmıştır. Birbirini izleyen altı geri dönüşümlü denemelerden sonra bile $CoO•CuFe_2O_4$ MMO ’ nun parçalama verimi oldukça yüksek olup TET ve EBT için sırasıyla ~ 93% ve 80% olarak ölçülmüştür.

Genel olarak, bu çalışmadan elde edilen bulgular $CoO•CuFe_2O_4$ MMO nun TET uzaklaştırılması işlemi için uygun bir adsorbent olabileceğini ve ayrıca sulu çözeltilerden EBT nin parçalanmasında ise uygun bir adsorbent/fotokatalist olabileceğini göstermiştir.

Anahtar kelimeler: fotokataliz, karışık metal oksitler, tetrasiklin, azo boyası, Eriochrome

ACKNOWLEDGEMENT

First and foremost, am grateful to God Almighty who made it possible for me to start and finish my PhD studies in EMU. It has not always been easy but your presence has always seen me through.

My sincere appreciation also goes to my supervisor, Prof Dr. Mustafa Gazi who not only acted as my academic supervisor but also as a mentor to direct me in all my research work during my PhD studies. Thanks hocam.

To my co-supervisor, Assoc. Prof. Dr. Akeem Oladipo, thanks for all the knowledge and information shared. I really appreciate everything and hope all yours plans in life come to fruition.

I would also like to thank and appreciate my jury members who took the pains of going through my PhD thesis write up, giving valuable inputs and suggestions that aided the completion of this study.

To my parents, brothers, sisters, nephews, nieces, Onos and in-laws, I want to say a massive thank you to you guys. You were all there for me when the going was tough. I dedicate this diploma to you all. I love you all.

Finally, I would like to appreciate everyone in the Department of Physics and Chemistry in EMU. From all my instructors (special mention to Prof. Dr. Elvan Yilmaz, Dr. Kivanc and Çilem Aydinlik) to my fellow research assistant colleagues (Basma, Meltem, Mamoon, Faisal, Cahit, Arwa, Selma) and friends (Abdullah,

Anthony, Edith, Khawla) at the department. I wish you guys all the best life has to offer. Gonna miss you all.

Not forgetting my family away from home; Stella Luki, Achiri Emmanuel, Roland, Lazarus. Thank you all for been good friends to me, I sincerely hope we achieve all we set out to achieve in life.

If no be God…….

TABLE OF CONTENTS

LIST OF TABLES

LIST OF FIGURES

Chapter 1

INTRODUCTION

1.1 Background study

The world at present is experiencing an unprecedented amount of water pollution as a result of exponential global population growth and unsupervised discharge of industrial wastes into the aquatic environment. In fact, ground and surface water in many regions around the world today are contaminated and unfit for human consumption (Gupta et al., 2012; Lee et al., 2015). As is well known, fresh and portable water plays an important role in our life and ecosystem today but this widespread pollution caused by rapid population growth, industries and human activities is raising serious social and economic concerns (Gupta et al., 2015).

According to a report by the United Nations Department of Economics and social Affairs, the global population is projected to be 9.6 billion by 2050 (UN report on world population prospects, 2013) and since the world's population and water resources are closely connected, it is predicted that at some point in the future there could be a crisis related to water scarcity and shortage (Gupta et al., 2012). The severity of this problem is evident in one of the biggest cities in the world today; Cape Town in South Africa which has a population of ~ 4 million (as at 2011 census) is facing severe water shortages and rationing (bbc.news.com; https://www.bbc.com/news/world-africa-42836560 accessed online August 10, 2019). Also, a World Health Organization report (2007) found that water scarcity

and pollution together with/or unsanitary living conditions resulted in the death of 12 million people yearly. This brings to the forefront the problem of water pollution and its impact on humans and the environment at large. All this has caused serious concerns for environmentalists and governments in different countries with research now geared towards detecting, accessing/monitoring water quality and finding cheap and affordable techniques to treat industrial effluents before it is discharged into the environment.

Azo dyes, a class of synthetic dyes containing –N=N– chromophore in their structure, constitute the largest and most extensively used dyes in the textile industry. In fact, they account for about 50% of the 700,000 tons of industrial dyes produced yearly worldwide for the textile industries with estimates showing that 10 - 15% of these dyes are discarded along with industrial wastewater, making them a major source of water pollutants (Karimi-Shamsabadi et al., 2017; Asad et al., 2007). Additionally, azo dyes are also used in cosmetics, food, paper and leather industries. The unsupervised discharge of dye effluents containing azo dyes and their metabolites into aquatic ecosystem impedes sunlight penetration which in turn has an adverse effect on photosynthetic activities thereby harming aquatic flora and fauna. Also, some of these dyes and their degradation products are toxic, mutagenic and carcinogenic in nature and may cause severe damage to humans (Saratale et al., 2011). Furthermore, persistent exposure to these azo dyes may result in severe skin irritation and respiratory problems. Even dye concentrations as low as 1.0 mg/L can make drinking water aesthetically unpleasing and unfit for human consumption (Crini 2006).

Eriochrome Black T; EBT is an azo dyestuff used in the textile industries for dyeing fibers, wool, silk, nylon etc. and as a complexometric indicator for determination of total hardness of water (Kansal et al., 2013). EBT is chemically stable, recalcitrant azo dye that is hazardous and poses several health hazards (such as eye irritation, nausea, vomiting etc.) to man and the aquatic biota (Kaur and Singhal., 2015; Lee et al., 2015). Consequently, there is an imperative need to find cheap and efficient ways to eradicate EBT from industrial waste water to the permissible level before discharge into environmental matrices.

Quite recently, another class of biologically active organic compounds has now been detected in trace amounts (ng/L-µg/L) in water sources. They are now widely referred to as '***emerging contaminants***' or '***emerging micro-pollutants***'. These organic compounds which include; pesticides, personal care products PCPs, illicit drugs, antidepressants, surfactants, pharmaceutically active compounds (PACs), endocrine disruptor compounds (EDCs) among others, are frequently discharged into the ecosystem which compensates for their rate of transformation and biodegradation, making them potential toxic pollutants in the aquatic environment (Alvares-Torellas et al. 2016; Akhtar et al., 2016; Bui et al., 2016).

Antibiotics, a class of PACs fall under this category since they are also widely used, continuously discharged and are detected in the environment in varying concentrations. A major route/pathway of these antibiotics into the ecosystem has been found to be via the sewage from pharmaceutical industries, hospitals, medical facilities, agricultural runoff and the improper disposal of expired or unused drugs (Yu et al., 2016). Subsequently, the presence of antibiotics in water even at low concentrations can result in development of antibiotic resistant strains which are

difficult to treat using conventional antibiotics, can cause skin disorders and could even pose potential threats to human health and aquatic life (Bajpal et al. 2012; Lai et al., 2009). As a result of the potential environmental risks posed by these compounds, several countries have imposed regulations to regulate their usage thereby limiting their impacts on the environment (Sarmah et al., 2006).

Tetracycline; TET is a broad spectrum, cheap antibiotic that is widely used by humans and animals as growth stimulators or to treat and prevent various diseases. TET is poorly metabolized *in vivo* (about 50–80%) and is readily excreted through urine and excrement either in the unchanged form or as its metabolites (Lian et al., 2013). Just like other antibiotics, several studies have confirmed the presence of TET in various environmental matrices such as; residential, industrial and agricultural waste streams (Lin et al., 2008), surface water and sediments from poultry slaughter house (Topal, 2015), waste water effluents (Watkinson et al., 2009) and even drinking water (Oladipo and Ifebajo 2018), hence just like EBT, it is also of great significance to eradicate TET from contaminated water supplies before discharge into the environment.

Many technologies (chemical, biological and physical) have been developed and reported for the removal of organic matrices such as synthetic dyes and tetracycline from aqueous matrices. In this regard, adsorption and heterogeneous photocatalysis have shown promising results. To date, various photocatalysts such as ZnO and TiO_2, low-cost adsorbents from agricultural wastes, biopolymers, clays etc. and composites (semi-conductors incorporated into polymers, biomaterials and agricultural wastes etc.) have been developed for removal of organic pollutants from aqueous solutions (Baccar et. al., 2010; Chieng et al., 2015; Gazi et al., 2017; Kim et al., 2017; Kansal et

al., 2013; Priya et al., 2016). Nevertheless, many of these techniques proposed are either costly, nonviable, photocatalysts may possess wide band gap coupled with rapid recombination of electron-hole pairs or could lead to the generation of secondary pollutants and toxic byproducts. Therefore, there is a need for new innovative ideas that would use a combination of established techniques to treat waste water effluents.

In line with this, we developed an efficient multifunctional material ($CoO•CuFe_2O_4$ MMO) that can act as an adsorbent and photocatalyst in waste water remediation. By using the magnetic MMO nanocatalyst, we were able to completely remove TET efficiently via adsorption and EBT via a combination of adsorption and sunlight assisted photodegradation. In addition, the kinetics, adsorption mechanism for both pollutants and probable photodegradation mechanism for EBT dye was proposed based on experimentally obtained results. Furthermore, the regeneration and reusability of the MMO was also evaluated.

1.2 Objectives/Aim of research work

The main objectives of this Ph.D. research work is to eradicate two model pollutants (an antibiotic; Tetracycline and azo dye; Eriochrome black T) using a $CoO•CuFe_2O_4$ mixed metal oxide.

The specific goal(s) of the Ph.D. project work are:

- To synthesize a multifunctional material that can act both as an adsorbent and photocatalyst in waste water remediation.
- Investigate the effects of several operational parameters including; pollutant initial solution pH, dosage, reaction contact time, radical scavengers etc. on

the removal of tetracycline via adsorption and Eriochrome black T via a combination of adsorption and photocatalysis.

- Systematically determine the adsorption capacity of $CoO•CuFe_2O_4$ MMO for both model pollutants under the investigated conditions.
- Carry out a detailed study of the experimental data to better understand the adsorption mechanism by using adsorption isotherms and kinetic models.
- Identify the main reactive specie RS responsible for the sunlight induced degradation of EBT and propose a mechanism for the degradation process.
- Finally, to compare the adsorptive and catalytic performance of the $CoO•CuFe_2O_4$ MMO with other adsorbents/photocatalyst previously reported in literature.

1.3 Thesis outline

The **first chapter** offers a brief introduction of the PhD research topic, the research goals, aims and objectives of carrying out the research and some limitations that could restrict the research studies while the **second chapter** gives a comprehensive literature review which will include; current knowledge, findings and shortcomings previously reported in literature by other researchers. **Chapter 2** emphasizes on the need to develop new adsorbents and/or photocatalysts to eradicate pollutants from aqueous solutions, emphasizing the advantages of using a combination of techniques (adsorption and heterogeneous photocatalysis) to deal with water pollution issues in the world today. **Chapter 3** will give a detailed experimental section including synthesis procedures, reagents and equipment used for reproducibility before all results obtained from the sample characterization, adsorption and photocatalysis experiments will be discussed extensively in the **fourth chapter**. Finally, **chapter 5**

will conclude and give recommendations based on the research work carried out in this PhD study.

1.4 Limitations of research study

This PhD thesis research study focused mainly on the application of the $CoO•CuFe_2O_4$ MMO under laboratory simulated conditions only. To fully determine the potential of the $CoO•CuFe_2O_4$ MMO synthesized, the adsorptive and catalytic potential of the $CoO•CuFe_2O_4$ MMO should be investigated using a wide range of pollutants including; heavy metals, more dyes (synthetic and natural) and several other micro-pollutants. Also, the efficiency of the $CoO•CuFe_2O_4$ mixed metal oxide should be investigated under a continuous system (i.e. for industrial application) or using real industrial wastewater containing either or both EBT and TET and/or any other model pollutant(s) in a single and multi-component pollutant system.

Chapter 2

LITERATURE REVIEW

2.1 Waste water remediation techniques

As earlier identified in the previous chapter, the presence of many environmental pollutants in water is raising serious health and environmental concerns worldwide. These toxic pollutants including but not limited to dyes, heavy metals, can cause serious threats to human health and the aquatic environment at large. Hence, the remediation of toxic pollutants from industrial wastewater to permissible limits before discharge and from wastewater treatment plants (WWTP) is extremely important. Technologies used in wastewater treatment (WWT) can be divided into three categories:

1. Biological methods: involves the use of microorganisms to treat industrial effluents. Very economical when compared to other technologies. However, industrial application on a large scale is limited due to technical constraints (Crini 2006).
2. Chemical methods: involves the use of chemical reagents to treat waste water. Process is often time expensive and could lead to secondary pollution via the accumulation of concentrated sludge.
3. Physical methods: include processes such as adsorption and membrane filtration. Is very cost effective and simple process. A major disadvantage is the periodic cost of replacing the membrane or adsorbents due to fouling.

The following paragraphs will briefly examine the treatment technologies available for WWT and reuse with more emphasis placed on adsorption and advanced oxidative processes AOPs.

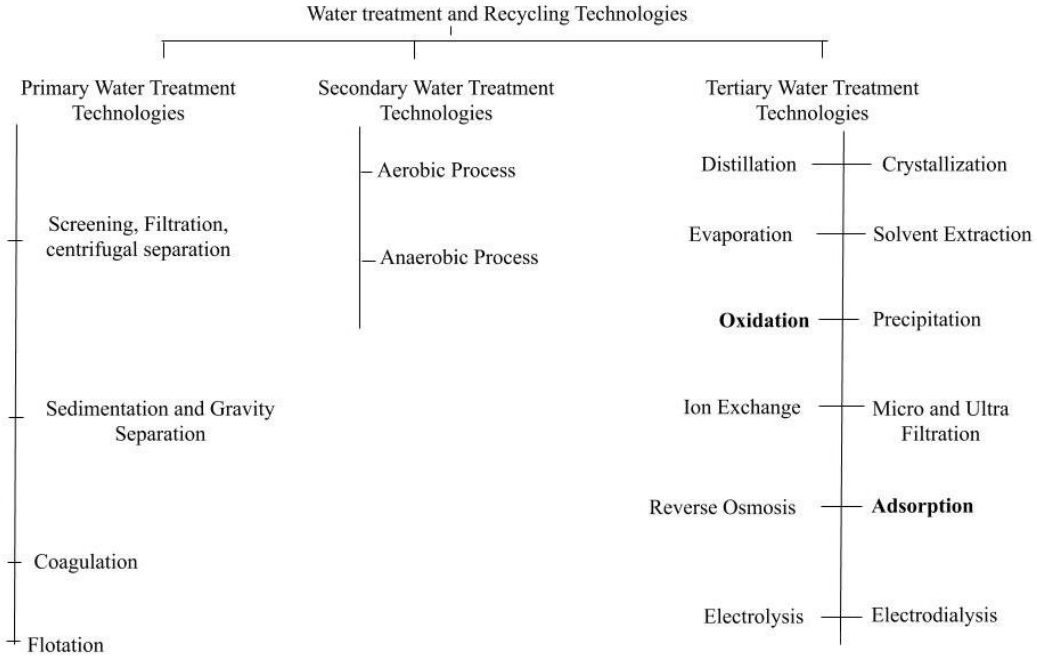

Figure 1: Water treatment and recycling technologies
Source: Gupta et al., 2012

According to the Figure above, there are three stages; primary, secondary and tertiary water treatment technologies combined together to produce good quality, safe water whereby 99% of pollutants are removed in a WWTP unit operation. The first stage which involves processes such as flotation, coagulation, filtration etc. is carried out when the water to be treated is highly polluted. Solid wastes, suspended solids, grits, oil and greases are removed in this stage. In the second stage, water is circulated in a reactor with high concentration of microbes. These microbes are responsible for the conversion of organic pollutants via aerobic or anaerobic processes. Finally, water safe for human consumption is produced in the final stage of the WWTP. The choice of water treatment technology used for WWT in the tertiary stage depends mainly on

the type of pollutant present and the final desired product i.e. water quality or requirements.

Generally, for economic reasons, care should be taken when selecting the required treatment technologies for WWT because these technologies depend on the source of the waste water, type of pollutant(s) present and the requirements of the final quality of water produced in the WWTP. For example, waste water low in Biochemical Oxygen Demand does not require secondary treatment process while ground water containing only metals can be treated directly using tertiary water treatment technology.

2.2 Advanced Oxidative Processes

Advanced oxidative processes AOPs constitute a promising technology for the treatment of bio-refractory organic contaminants in wastewater based on the *in situ* generation of a non-selective highly reactive oxidant; hydroxyl radicals ($OH^{\bullet}$) with strong oxidizing capacity that are capable of attacking chemicals bonds present in organic compounds. Conventional AOPs are able to break down complex organic molecules into smaller organic compounds or in some cases completely mineralize them into harmless inorganic products such as carbon dioxide and water at ambient temperatures and pressure (Wang et al., 2016). AOPs can be classified according to the; (i) means of generating the ($OH^{\bullet}$) radical either through chemical or otherwise, or (ii) the reactive phase (homogeneous and heterogeneous). The main difference between the homogeneous and heterogeneous reactive phase is that while the catalytic process always takes place on the catalyst surface in the latter, it occurs in the liquid phase for the former (Babuponnusami and Muthukumar, 2013).

Numerous studies have reported the use of a wide range of AOPs to treat different organic pollutants under laboratory conditions with certain degree of success (Priya et al., 2016; Oladipo 2018; Di et al., 2017; Duarte et al., 2009; Ferkous et al., 2016). Although AOPs have many advantages such as; ease of operation and low cost, high performance coupled with the ability to treat highly contaminated and toxic wastewater etc. over other conventional methods, some limitations like generation of toxic intermediates and production of large volumes of toxic sludge have limited their overall industrial applications (Priya et al., 2016). Examples of AOPs are, Fenton and Fenton-like reactions, sonolysis, UV photolysis, Ozonation, photocatalysis, etc. Also, some of these methods could also be combined together to maximize the degradation process and potential of the AOP e.g. Electro-Fenton, UV/ozone, Photo Fenton and photo Fenton-like reactions, Sono-Fenton, UV/photocatalysis etc. However in this study, two of the most widely used AOPs will be discussed below.

2.2.1 Fenton, Fenton-like and Photo-Fenton reactions

One of the most widely used AOPs is the Fenton process. The classical Fenton process involves the generation of hydroxyl radicals (OH•) that are capable of attacking recalcitrant organic compounds from soluble iron salts (Fe^{2+}) and an oxidant (usually hydrogen peroxide) according to Eq. (1) and (2).

$$Fe^{2+} + H_2O_2 \rightarrow Fe^{3+} + OH^- + HO^{\bullet} \quad (1)$$

$$Fe^{3+} + H_2O_2 \rightarrow Fe^{2+} + H^+ + HO_2^{\bullet} \quad (2)$$

The OH• radicals generated have a strong oxidizing potential ($E° = +2.80\ V_{NHE}$) whereby they can abstract hydrogen atoms from organic compounds to produce an organic radical which subsequently undergoes a sequence of chemical reactions to break down the organic compound into smaller less harmful substances (Rauf et al.,

2011). Some advantages of the Fenton process over other AOPs are; high performance and design simplicity, non-toxicity and process efficiency. Despite these advantages, a major drawback of the process is the generation of large amount of sludge coupled with high metal concentration in the final effluent (50-80 ppm). Also, the process can only be carried out in limited range of pH usually in the acidic medium (Duarte et al., 2009). Thus, the Fenton-like reaction (Heterogeneous Fenton) which uses solid-liquid interface reaction has proven to be an effective means of circumventing this problem (Gu et al., 2013). For this purpose, various ferrous ions supports like resins, activated carbon, clay, silica, zeolites etc. have been used to synthesize novel heterogeneous Fenton catalysts. Additionally, some non-iron Fenton catalysts which include elements with multiple oxidation states have been discovered. These elements can all directly decompose hydrogen peroxide via Fenton-like reactions to produce hydroxyl radicals *in situ* even at neutral pH (Bokare and Choi, 2014).

In the photo Fenton-like process, the Fenton reaction is carried out under solar or ultraviolet light irradiation. This helps to improve the oxidation efficiency of the process by enhancing the overall production of $OH^{\bullet}$ radicals according to the reactions shown below;

$$H_2O_2 + h\nu \rightarrow 2\ HO^{\bullet} \quad (3)$$

$$Fe(OH)^{2+} + h\nu \rightarrow HO^{\bullet} + Fe^{2+} + H^{+} \quad (4)$$

This process is advantageous because it reduces the iron waste produced as sludge, regenerates Fe^{2+} ions needed in the breakdown of H_2O_2 and also enhances the decomposition of hydrogen peroxide into $HO^{\bullet}$ radicals required for the degradation process.

2.2.2 Heterogeneous photocatalysis

Photocatalysis is one of the green, sustainable and emerging technologies for WWT. It involves the use of light sensitive semiconductors such as TiO_2, ZnO, CdS, PbS etc. for degrading and completely mineralizing some environmental pollutants (Rauf et al., 2011). In this process, light energy from any source (either UV or visible light) that is higher than or equal to the band gap energy of the catalyst excites electrons from the valence band to the conduction band of the photocatalyst before a series of chemical reactions result in the formation of $HO^{\bullet}$ radicals and some other reactive species which are capable of degrading organic pollutants (Gupta et al., 2012).

TiO_2 and ZnO nanoparticles are two of the most well-known and widely used semiconducting photocatalysts in industries and laboratories till date, however, both possess a wide band gap (3.2 eV for TiO_2 and ~3.3 eV for ZnO) meaning they can only be excited in the UV region and low efficiency due to the rapid recombination of their photogenerated electron-hole pairs which limits their industrial application (Gazi et al., 2017; Di et al., 2017). Therefore, in order to improve their properties and exploit visible light in the solar spectrum (52%), there is a need to develop catalysts with improved properties that can perform efficiently under sunlight irradiation.

A common strategy used to improve the properties of TiO_2 or ZnO is by doping them with metals such as Co, Fe, Mn, Cr etc. so as to inhibit the fast recombination of the electron-hole pair and adjust the band gap towards the visible region (Kim et al., 2017; Rauf et al., 2011). Also, hybrid nanocomposites can be developed by combining these light sensitive semiconductors with different supports such as LDHs, activated carbon etc. or in other cases, completely new catalysts can be

synthesized using a combination of different metals as shown in this thesis work (Prasad et al., 2019; Gazi et al., 2017).

To date, there are reports on the removal of EBT dye but no attempt has been made to the best of our knowledge to investigate the degradation of EBT using a $CoO•CuFe_2O_4$ mixed metal oxide obtained from Co-Cu-Fe LDH as a heterogeneous catalyst.

2.3 Adsorption

Adsorption technique is one of the physical methods currently applied for the removal of a wide range of pollutants from wastewater. It is a relatively simple process that involves the transfer of adsorbate molecules, ions and atoms from the bulk solution phase onto the surface of an adsorbent without generating any toxic intermediates (Oladipo and Ifebajo, 2018). Table 1 shows some advantages and drawbacks associated with the adsorption process.

Table 1: Advantages and disadvantages of adsorption

Advantages	Disadvantages
• Cheap process requiring low capital investment. • Relatively simple process to carry out i.e. Simplicity of design. • Insensitive to toxic wastes and pollutants. • Very efficient for various pollutants. • Low energy cost/ energy saving. • No generation of toxic by-products or intermediates. • Availability of a wide range of adsorbents that can easily be modified to improve its potential.	• Is non-destructive in nature and leads to the generation of secondary pollution. • Ineffective against some contaminants. • Regeneration of adsorbents can be quite expensive and adds to the overall cost of the process. • Pretreatment of waste water is usually required to remove oils and suspended particles that could affect the efficiency of the adsorbents.

Commercial Activated carbon (AC) has been widely used on an industrial scale in WWTPs due to their structural properties, high surface area and porous texture. However, the cost of production and desorption/regeneration of AC have led to several attempts by researchers worldwide to find cheaper means of producing AC or more effective alternatives (Crini 2006). To this end, the potential of many low cost adsorbents have been studied and proposed as suitable replacements for AC in WWT. They include but are not limited to: wastes from agricultural materials and industries, biopolymers, clays, metal organic frameworks (MOFs), metal oxides (Ifebajo et al., 2019; Tang et al., 2012; Ben-Ali et al., 2017; Hazzaa and Hussein, 2015; Baccar et al., 2010).

Even though many studies have been carried out on the removal of TET antibiotic via adsorption in single and/or binary systems, both in my doctorate research work and by other researchers with varying degree of success (Ersan 2016; Li et al., 2012; Marzbali et al., 2016; Oladipo et al., 2017; Oladipo and Ifebajo, 2018; Ifebajo et al., 2019), we did not find any research work related to the use of $CoO{\bullet}CuFe_2O_4$ MMO for the removal of TET.

2.3.1 Factors affecting adsorption

As is well known, the adsorption process is affected by a wide range of experimental factors. All this factors needs to be carefully investigated so as to determine the optimum conditions for adsorptive removal of each pollutant. One very important factor that is considered in most studies of adsorption is solution pH. This is because the pH not only affects the surface properties of some adsorbents e.g. the degree of ionization and surface charge, it can also determine the properties of the pollutants as well (Mahmoud et al., 2016). For example TET has different speciation based on solution pH due to its ***Pka*** values while EBT exhibits different colors in the acidic

and basic media. Ersan (2016) and Chieng et al. (2015) found that maximum adsorption of TET and Rhodamine B dye by polypropylene polystyrene biocomposites and peat was observed at pH 6.0 and 3.0 respectively. This behavior was alluded both to the surface chemistry i.e. pH_{pzc} of the materials and the pH dependent nature of both pollutants (Ersan 2016; Chieng et al., 2015).

Adsorbent dosage and solution temperature also has a vital role to play in the removal efficiency of any adsorbent. An increase in adsorbent dosage in most cases result in a corresponding increase in the removal efficiency up to a point. Rani et al. (2015) reported that the removal efficiency of safranin dye by surface modified carbonized *Eichhornia crassipes* increased from 68–99% as dosage increased from 0.25–1.5 g. A further increase in dosage had minimal impact on the adsorption process. It was implied that the dosage increase created more binding sites for safranin molecules (Rani et al., 2015). An increase in temperature on the other hand could either favor (endothermic process) or inhibit (exothermic process) the adsorption process (Foo and Hameed, 2012; Sen et al., 2011).

Another factor that could affect adsorption is particle size. Some studies have shown that decreasing the adsorbent particle size increased its adsorption capacity and reduced equilibrium sorption time (Ben-Ali et al., 2017; Preethi et al., 2006; Barka et al., 2013). A probable explanation for this is that as the particle size of adsorbents decreased, the surface area and readily accessible sites on adsorbent surface increased which invariably resulted in rapid rate of adsorption (Aksu et al., 2015). Other factors include that affects adsorption are; ionic strength, coexisting or counter ions in solution, reaction contact time, salinity, contact time and the presence of other contaminants in solution.

2.3.2 Kinetics and Isotherm studies

Adsorption isotherms

To date, different equilibrium isotherm models have been proposed and formulated to explain the mechanism involved in adsorption processes. However, in this study, we will briefly review four commonly used isotherms to predict the interaction between the mixed metal oxide synthesized and both model pollutants chosen for this thesis work. Comparative studies and analyses of adsorption equilibrium isotherm are very useful in predicting the capacity of an adsorbent for a particular adsorbate. Also, some parameters obtained from these adsorption isotherm equations can give valuable information about the surface properties of the adsorbent and its affinity towards the adsorbent. The non-linear and linear forms of the four two-parameter isotherms employed in this study are presented in Table 2.

The applicability of the adsorption isotherm equations to the experimental data was achieved by comparing the correlation coefficient (R^2) values and validated using two error functions (Chi-square test and normalized standard deviation).

Table 2: Linear and non-linear adsorption isotherm equations

Isotherms	Non-linear	Linear	Description
Langmuir	$q_e = \frac{K_L C_e q_{max}}{1 + K_L C_e}$	$\frac{1}{q_e} = \frac{1}{K_L q_m C_e} + \frac{1}{q_m}$	q_e, C_e, K_L, q_{max} represent equilibrium uptake capacity (mg/g), equilibrium concentration of pollutant (mg/L), Langmuir constant (L/mg) and maximum monolayer adsorption capacity (mg/g).
Freundlich	$q_e = K_F C_e^{1/n}$	$In\ q_e = In\ K_F + {}^{1}/_{n}\ In\ C_e$	q_e, C_e, are the equilibrium uptake capacity (mg/g), equilibrium concentration of pollutant (mg/L) and K_F and *1/n* are Freundlich's constant related to bond energies and adsorption intensity.
Temkin	$q_e = \frac{RT}{b_T}\ In\ K_T C_e$	$q_e = B\ InA + B\ In\ C_e$ $B = \frac{RT}{b_T}$	B, A, R, T and b_T are the heat of adsorption (KJ/mol), equilibrium binding constant (L/mg), universal gas constant (8.314 J/mol K), absolute temperature (K) and Temkin isotherm constant.
Dubinin-Radushkevich (D-R)	$q_e = q_{max}^{\exp(-\beta\varepsilon^2)}$	$In\ q_e = In\ q_m - \beta\varepsilon^2$ $\varepsilon = RT\ In\ (1 + \frac{1}{C_e})$ $E = \frac{1}{\sqrt{2\beta}}$	q_m, β, E, ε represent the theoretical saturation capacity (mg/g), D-R constant, mean energy of sorption and the Polanyi potential.

The Langmuir isotherm proposed by Langmuir (1918) is perhaps once of the best known and widely applied adsorption isotherm used to describe adsorption mechanisms (Langmuir 1918). This isotherm was originally designed to describe the adsorption of gas unto activated carbon but has now been applied for several adsorbent-adsorbate systems. The Langmuir empirical model proposes homogeneous adsorption surface signifying a monolayer adsorption that can only occur at a fixed/finite number of active sites on adsorbent surface with uniform energy. It also assumes that each active site on the surface of the adsorbent possesses equal attraction for adsorbate molecules and that there is no interaction and steric hindrance between adsorbate molecules even when they are on adjacent sites (Foo and Hameed, 2010).

Another widely applied adsorption isotherm is the Freundlich isotherm equation. This model was originally developed for the adsorption by animal charcoal (Freundlich 1906). The Freundlich empirical model is quite different from the Langmuir model in that it assumes adsorption process to occur via a multilayer adsorption over the surface of a heterogeneous adsorbent and that there is interaction between adsorbate molecules (Ben-Ali et al., 2017). The actives sites on the adsorbent are assumed to have a non-uniform distribution of heat and affinity towards the adsorbate molecules. In this case, sites with stronger binding energy and higher affinity towards the adsorbate molecules are first occupied until the adsorption energy decreases exponentially upon the completion of the adsorption process (Foo and Hameed, 2010).

The Tempkin isotherm model is originally used to describe the adsorption of hydrogen on platinum electrodes in acidic solutions (Foo and Hameed, 2010). This

model suggests that there is and considers the impact of an indirect interaction between adsorbent-adsorbate molecules on the adsorption process. The model also assumes that the adsorption process is characterized by a uniform distribution of binding energies up to some maximum binding energy and that the heat of adsorption of all adsorbate molecules decreases linearly and not logarithmic as the surface of the adsorbent is covered due to this said interactions (Hazzaa and Hussein, 2015; Barka et al., 2013).

The Dubinin-Radushkevich isotherm model was originally devised for the adsorption of subcritical vapors on microporous solids following a pore-filling mechanism and indicates adsorption over a heterogeneous surface with a Gaussian energy distribution (Dabrowski 2001; Foo and Hameed, 2012). This model was often times applied to differentiate the chemical and physical nature of the adsorption process in metal ions (Altin et al., 1998). The values of the mean biosorption energy, E helps to distinguish if the adsorption process is chemical (E>8 KJ/mol) or physical (E<8 KJ/mol) in nature.

Adsorption kinetics

Kinetic adsorption studies not only provide valuable information about the mechanism controlling the adsorption process and rate of pollutant uptake at the solid-solution interface, they are also important in the design of batch adsorption systems and identifying optimum operating conditions for full-scale batch operations (Barka et al., 2013). In this thesis work, four kinetic models were applied to further predict the adsorption mechanism. The linear forms of these equations are presented in Table 3.

Table 3: Linear and non-linear equations of kinetic models for adsorption process

Kinetic models	Linear	Description
Pseudo-first-order (P.F.O)	$In\ (q_e - q_t) = In\ q_{exp} - K_{FO}t$	K_{FO}, q_e, q_t and q_{exp} are the P.F.O rate constant (min^{-1}), equilibrium uptake (mg/g), uptake at time t (mg/g) and model calculated equilibrium sorption uptake.
Pseudo-second-order (P.S.O)	$\frac{t}{q_t} = \frac{1}{K_{SO}{q_{exp}}^2} + \frac{t}{q_{exp}}$	q_e, q_t and q_{exp} similar as P.F.O model above while K_{SO} is the P.S.O rate constant (g/mg min^{-1})
Elovich	$q_t = \alpha + \beta\, In\, t$	α and β are the initial sorption rate (mg/g min) and desorption constant related to the extent of surface coverage (g/mg) respectively.
Intraparticle diffusion	$q_t = K_{IP}t^{0.5} + C$	K_{IP} is the intraparticle diffusion rate constant and C is a constant related to thickness of the boundary layer.

The P.F.O model equation first proposed by Lagergren (1898) was originally used for the adsorptive removal of malonic and oxalic acid by charcoal (Tran et al., 2017). This model is well suited to explaining the adsorption process in solid-liquid systems and assumes a physical adsorption process whereby the rate of change of adsorbate uptake capacity with time is directly related to the difference in the concentration saturation level while the P.S.O model which was introduced by Ho and McKay (1998), assumes that chemisorption, involving covalent chemical bonds or valence

forces (i.e. exchange or sharing of electrons) may be the rate-determining step in the adsorption process (Ben-Ali et al., 2017; Oladipo et al., 2014; Rani et al., 2015). The Elovich model on the other hand is also used to describe second-order-kinetics and assumes the actual surface of the solid adsorbent to be energetically heterogeneous (Bajpai et al., 2012).

Adsorption which is a multi-step process involves the transport of adsorbate or solute molecules from the liquid phase onto a solid adsorbent is usually characterized by several steps involving external mass transfer, intraparticle diffusion or a combination of both processes (Wang and Wu, 2006). Hence, the overall adsorption process can be described by the three consecutive steps outlined below:

- The transport of the adsorbate molecules from the bulk solution through a liquid film to the external surface of the adsorbent i.e. boundary layer or film diffusion.
- Diffusion of adsorbate molecules into the pores of the adsorbent i.e. pore/intraparticle diffusion.
- Adsorption of the adsorbate molecules into the active sites on the interior surfaces of the pores of the adsorbent.

The intraparticle diffusion based on a theory formulated by Weber and Morris (1963) as compared to other kinetics models discussed above is used to determine the mechanism of adsorption and identify the plausible rate-determining step affecting the kinetic process. Ideally, for intraparticle diffusion to be the one and only rate-controlling step, the plot of adsorbate uptake, q_t with respect to the square root of time must be linear over the entire time range studied if not, the overall adsorption

process is said to be controlled by a combination of more than one step such as ion exchange, complexation etc. (Barka et al., 2013).

2.4 Layered double hydroxides

Layered double hydroxides; LDHs are two-dimensional hydrotalcite-like ionic clay compounds with highly tunable brucite structures that have been studied extensively because of their versatility and numerous potential applications in many fields (Zubair et al., 2017a). The chemical composition of LDHs can be expressed using the general formula $[M_{1-x}^{2+}M_x^{3+}[OH]_2)^{x+}(A_{x/n}^{n-})^{x-}\cdot mH_2O]$ where M^{2+}, M^{3+}, A^{n-} in the formula represent the divalent, trivalent cations and interlayer/exchangeable anion respectively while x is the molar ratio i.e. $M^{3+}/M^{2+}+M^{3+}$ (Lu et al., 2016).

The use of LDHs, LDH composite (LDH-C) and LDH containing hybrids (LDH-H) either as adsorbents or catalysts in AOPs is now gaining significant attention in wastewater remediation due to their non-toxicity, large surface areas, low cost, good thermal stability, highly tunable structure and exchangeable anionic capacity coupled with excellent sorption capacities and regeneration potential (Mahjoubi et al., 2017; Zubair et al., 2017a).

To date, a variety of LDHs have been reported as potential adsorbents for water purification. Ling and co. synthesized a novel CoFe LDH and applied it for the removal of methyl orange and Cr(VI). They found that the CoFe LDH exhibited a fast removal of Cr(VI) at initial concentration of 2–25 mg L^{-1} within 5 min and high adsorption capacity of 1290 mg g^{-1} for methyl orange (MO) at an initial dye concentration of 300 mg L^{-1} (Ling et al., 2016). MgAl and MgFeAl LDH were prepared from facile co-precipitation method and used for the effective capture of

uranium; U(VI) from saline lake brine. The LDHs were found to have a high affinity towards U(VI) which was more than twice that observed by other LDH based materials (Tu et al., 2019). Zn-Al LDHs intercalated with several anions were synthesized and applied for the removal of MO via adsorption. The results obtained from this study showed that pH was the most influencing factor in the removal process while the Zn-Al LDH containing sulfate ions exhibited the highest adsorption capacity of 2758 mg/g (Mahjoubi et al., 2017). Mg-Al-CO_3 LDHs were also prepared and used for the removal of three dyes (reactive red, congo red and acid red 1) via batch adsorption process. All three dyes were effectively removed by the as-synthesized LDH at optimum dosage and contact time of 100 mg and 60 min respectively. Also, they found that the dye solution pH (pH < 10) had little impact on the adsorption process (Shan et al., 2015).

Recently, LDH used either as catalyst or catalyst support systems (LDH-C and LDH-H) is also receiving more and more interest from researchers in the field of AOPs. The performance of several Photocatalytic Zn/M-NO_3 LDHs (M = Al, Fe, Ti and Fe/Ti) for the visible-light driven degradation of Rhodamine B dye (RB) was tested. Zn/Ti LDH showed the highest degradation of 98 % for RB after 120 min while the degradation kinetics was well fitted to the pseudo-first order kinetic model (Xia et al., 2013). Similarly, ZnTi LDH with varying Zn/Ti ratios displayed significant photocatalytic potential towards the visible light driven degradation of methylene blue MB (initial concentration of $1.6*10^{-5}$ M) with ~ 100% removal observed after 100 min reaction time (Shao et al., 2011). Magnetite/CoCr LDH composite was evaluated both as an adsorbent and catalyst for the degradation of reactive black dye via Fenton-like and photo Fenton-like reactions. The LDH composite was found to

be more efficient than the LDH due to its larger pore size and surface area (Goncalves et al., 2019).

Another new and interesting field with promising results is the use of LDHs, its nanocomposites and hybrids as antibacterial agents and in biomedical applications such as gene and drug delivery vehicles (Nejati et al., 2015; Rasouli et al., 2017; Sun et al., 2017; Ladewig et al., 2010; Rives et al., 2014). All this proves to show that LDHs have a wide range of applications in many fields.

LDHs can readily be transformed via microwave treatment or thermal decomposition (heating at high temperatures) to form their corresponding metal oxides (Figure 2). These mixed metal oxides (MMOs) possess relatively higher surface area, good structural memory effect, chemical and thermal stability, stronger alkalinity, high dispersion at atomic level, improved catalytic property and higher anion exchange capacity than their LDH precursors which makes them also a promising alternative as solid adsorbents and heterogeneous photocatalysts for waste water decontamination (Jawad et al., 2015; Deng et al., 2016; Di et al., 2017).

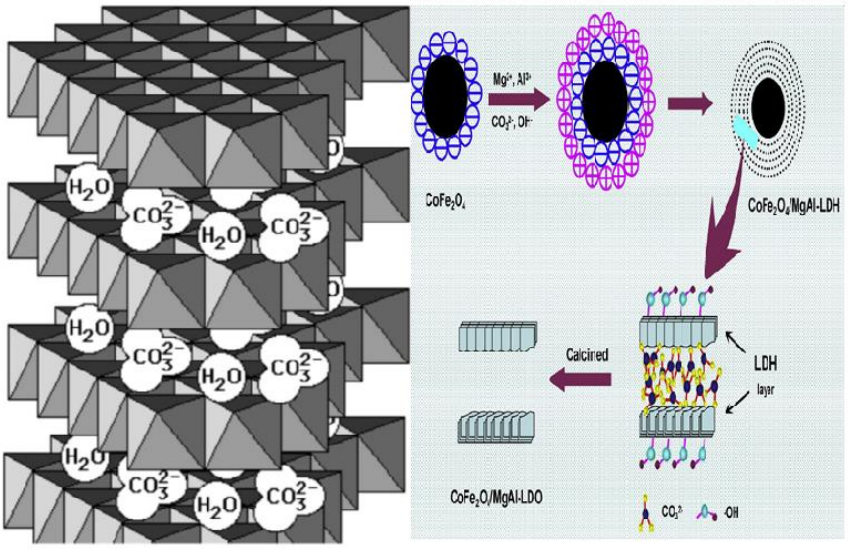

Figure 2: (a) LDH intercalated with CO_3^{2-} ions and water molecules and (b) conversion of MgAlLDH to $CoFe_2O_4$/MgAl MMO via calcination
Source: (a) Rives et al., 2014 (b) Deng et al., 2016

MMOs just like corresponding LDHs are also attracting considerable attention in the field of waste water treatment due to the reasons stated above. In fact, some studies comparing the adsorptive efficacy of both MMOs and LDHs for removal of several pollutants from aqueous solutions have found that MMOs usually display relatively higher adsorption capacities than their corresponding LDH precursors (Lei et al., 2017; Yao et al., 2017). Zubair et al., (2017b) reported an efficient adsorption of EBT from aqueous phase by MgAl–, CoAl– and NiFe– calcined LDHs with maximum adsorption capacities of 419.87, 540.91 and 132.49 mg/g respectively. Many other reports have also studied the adsorption of metals, dyes and different contaminants using MMOs with a high degree of success recorded (Huang et al., 2017; Lee et al., 2018; Hu et al., 2018).

MMOs have also been widely reported as catalyst in waste water remediation. A few of these studies will be discussed. Di et al. (2017) synthesized a series of Zn-Fe MMOs and applied them for the simultaneous removal of arsenic and several

pharmaceuticals via a combination of adsorption and photocatalysis. Mechanistic studies revealed that the photogenerated holes in the Zn-Fe MMOs played a major part in the degradation process while the presence of ibuprofen had no obvious impact on the removal of arsenic (Di et al., 2017). Another study reported in literature found that doping ZnAl MMOs with Cu and Co ions enhanced their photocatalytic ability towards the degradation of Orange II dye under UV irradiation (Kim et al., 2017). CoMnAl MMOs were synthesized and employed for the catalytic degradation of Bisphenol A (BPA) through the heterogeneous activation of Potassium peroxymonosulfate (Oxone). The results indicated that sulfate radicals ($SO_4^{-\bullet}$) were the main oxidizing specie in the process and that the combination of the CoMnAl MMO and Oxone presented considerably high removal efficiencies for the degradation of BPA (Li et al., 2015). Interestingly, a study a carried out by our research group found that CoO–$NiFe_2O_4$ MMO exhibited good catalytic potential for the removal of EBT dye via heterogeneous Fenton-like and sonocatalytic reactions (Oladipo et al., 2019). Finally, just like their LDH precursors, MMOs have also been applied for various biomedical and antibacterial studies (Raghunath and Perumal 2017; Carbone et al., 2017).

The brief review of literature undertaken in this chapter identifies the massive potential of adsorption and AOPs in WWT facilities. However, due to the different physiochemical properties of pollutants in water, a combination of two or more established water treatment techniques have been suggested as a potential strategy in WWT and WWTPs. From these studies, we found that most adsorbents do not possess light sensitive properties while most catalysts cannot effectively act as good adsorbents or can only function well under UV light. This makes it difficult to find materials that can act both as adsorbents and photocatalyst. Hence, to address these

shortcomings, we prepared a multifunctional material that has both good adsorptive and photocatalytic properties under UV and visible light irradiation.

Chapter 3

EXPERIMENTAL SECTION

3.1 Materials and Chemical reagents

Every chemical reagents used in this study were of analytical grade (< 99.9%). Deionized water was also applied as a solvent to prepare all solutions. Model pollutants Tetracycline; (TET; $C_{22}H_{24}N_2O_8$; Mol. Wt. 444.43 g mol^{-1} and Eriochrome Black T (EBT; $C_{20}H_{12}N_3NaO_7S$; Mol. Wt. 461.38 g mol^{-1}) was supplied by Merck, Germany; sodium hydroxide (NaOH) and $Co(NO_3)_2.6H_2O$ were purchased from Aldrich (Germany). $Cu(NO_3)_2.3H_2O$ and Fe $(NO_3)_3.9H_2O$ was acquired from Carlo Erba reagents (Spain). All solution pH(s) were determined using a HANNA HI 98127 laboratory pH meter while sample calcination was achieved with the aid of a muffle furnace (Nabertherm GmbH model). The concentration of both pollutants (i.e. TET and EBT) remaining in solution was analyzed with the aid of a T80+ UV-vis spectrophotometer (PG instruments Ltd., United Kingdom).

3.2 Synthesis of LDH and mixed metal oxide MMO

The synthesis of $CoO•CuFe_2O_4$ MMO was carried out in two stages as reported in our study (Ifebajo et al., 2018). Briefly, a solution containing Co^{2+} and Fe^{3+} ions (1:1 molar ratio) was prepared by dissolving the required amount of $Co(NO_3)_2.6H_2O$ and Fe $(NO_3)_3.9H_2O$ in 0.05 L deionized water. The solution was then carefully added dropwise under constant stirring using a peristaltic pump (1 mL/ minute) into an aqueous solution of sodium hydroxide (0.4 moles) at room temperature (25 ± 1 °C) until a pH ~ 9.0 to produce the cobalt iron layered double hydroxides; Co•Fe LDH.

After stabilizing at the desired pH, the dark brown precipitates of Co•Fe LDH obtained was then aged in the mother liquor for 24 hours at 65 °C before centrifugation (2000 rpm for 15 minutes), washing severally with distilled water and drying in an oven at 80 °C until a constant mass was achieved.

In the second stage, 5 grams of the synthesized Co•Fe LDH was weighed into a 250 mL beaker containing an aqueous solution of $Cu(NO_3)_2.6H_2O$ (65 mM) and vigorously stirred at ambient temperature for three hours. The product (Co-Cu-Fe LDH) was filtered, washed using an ethanol-water mixture (1:1) and dried overnight in the oven at 60 degrees. Afterwards, the Co-Cu-Fe LDH was calcined in the furnace at 500 °C (ramp heating rate set at 10 degree/minute) for five hours before cooling to ambient temperature. The final product; $CoO•CuFe_2O_4$ MMO was ground into fine powder and stored inside sealed glass bottles awaiting further use.

3.2 Sample characterization

Textural measurements to determine the specific surface area (SSA) and pore size distribution of both Co•Fe LDH and $CoO•CuFe_2O_4$ MMO were obtained by using a Quanta Chrome autosorb analyzer to determine the nitrogen adsorption-desorption isotherms at 77 K. The pore distribution and SSAs of the Co•Fe LDH and $CoO•CuFe_2O_4$ MMO were then calculated using the Brunauer-Joyner-Hallenda (BJH) and Brunauer-EmmettTeller (BET) equations respectively. FTIR spectra of both samples were obtained with the aid of a 8700 Perkin Elmer FTIR spectrophotometer (wavenumber range and resolution: 4000 – 400 cm^{-1} and 4 cm^{-1}). Surface morphology and chemical compositions of both Co•Fe LDH and $CoO•CuFe_2O_4$ MMO were observed with the aid of a scanning electron microscope (JSM-6390 JEOL, Japan) fitted with a detector for the EDX (energy dispersive X-

ray) analysis. Thermogravimetric analysis (TGA) of both samples was undertaken at heating rate of 10 degree/min under inert conditions with a TA thermal analyzer system (STA 7300, HITACHI). A VSM, 7400-S vibrating scanning magnetometer was applied at ambient temperature to check the magnetic properties of the Co•Fe LDH and $CoO•CuFe_2O_4$ MMO while a Shimadzu UV-2450 spectrophotometer was used to identify the optical properties of both samples. A diffractometer (D-8 Advance) operated at wavelength of 1.542 Å and 40 KV was used to record the power XRD patterns (angular range 2Θ over 10-80° with 2 sec/step) of both LDH and MMO samples respectively. The crystalline phases of the samples were then identified from the JCPDS files.

The point of zero charge (pH_{pzc}) of the $CoO•CuFe_2O_4$ MMO was also investigated using the pH drift method. Briefly, 200 mg of the $CoO•CuFe_2O_4$ MMO was added to several beakers containing 0.05 L of 0.1 mol/L NaCl (initial pH value of sodium chloride solution were already adjusted from pH 1-10) and agitated for 48 hours. Thereafter, the final solution pH was taken and the pH_{pzc} was obtained as the point of intersection from a plot of the initial solution pH and final solution pH.

3.3 Batch adsorption study of Tetracycline and Eriochrome Black T

Batch experimental adsorption studies were undertaken to assess the capacity of the $CoO•CuFe_2O_4$ MMO to adsorb both EBT and TET from waste water under laboratory conditions. For each experimental run, 50 mg of adsorbent was added to 0.05 L aqueous pollutant solutions of varying initial concentrations in 250 mL conical flasks and agitated at 250 rpm using a temperature controlled shaker at room temperature. A blank run containing only the pollutant in the conical flasks without the adsorbent i.e. $CoO•CuFe_2O_4$ MMO was also shaken simultaneously. This was

done to determine if any adsorption occurs on the walls of the conical flask. The initial solution pH of EBT and TET solution(s) were adjusted using 0.1 mol/L base (sodium hydroxide) and acid (HCl) without buffering.

At predetermined time intervals, the CoO•$CuFe_2O_4$ MMO was separated from the reaction solution with the aid of an external magnet before 1 mL aliquots of the mixture were taken to determine the residual TET or EBT concentration in solution phase with a UV-Vis spectrophotometer at Λ_{max} = 354 and 530 nm for TET and EBT. The amount of pollutant absorbed (q_e) and extent of degradation/removal percentage was calculated using Eqs. (5) and (6);

$$q_e = (C_1 - C_2)\frac{V}{M} \tag{5}$$

$$\%\, removal = \left(\frac{C_1 - C_2}{C_1}\right) * 100 \tag{6}$$

Where C_1 and C_2 in ppm are the initial and final TET and EBT concentrations, V represents the volume of TET and EBT solution (Liters) and M is the mass of CoO•$CuFe_2O_4$ MMO in grams. To ensure reproducibility of results, all sorption experiments were repeated in duplicates with the average values reported.

Stock solutions (1000 ppm) of both TET and EBT were obtained by dissolving the appropriate amount of each pollutant in 1L deionized water. Serial dilutions of the already prepared stock solution were obtained to prepare the needed pollutant concentrations (i.e. working solutions). The standard Calibration curves for both pollutants were plotted and are presented in Fig 3.

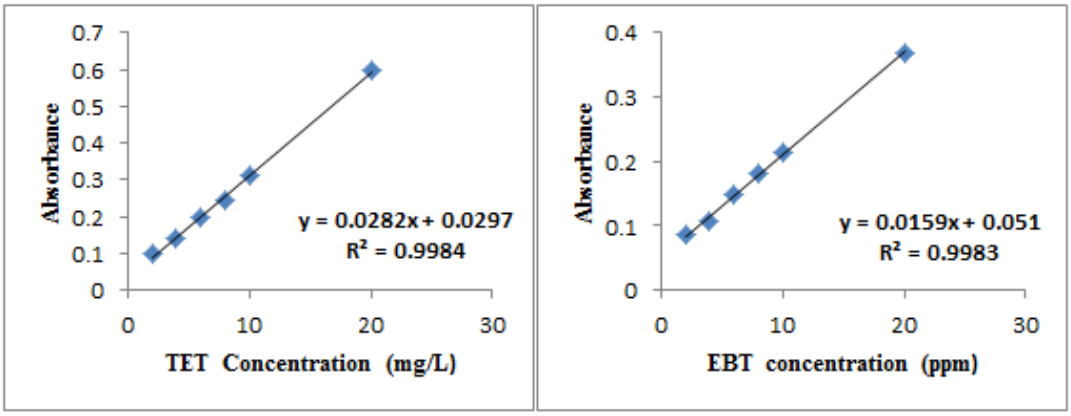

Figure 3: Calibration curves for TET and EBT

3.4 Sunlight assisted degradation of Eriochrome Black T

Photocatalytic degradation experiments of EBT dye using the $CoO•CuFe_2O_4$ MMO catalyst were carried out under direct solar light irradiation from 10:00 – 15:00 hours during the months of April and June 2018. The initial solution pH of the dye solution was adjusted to the appropriate pH with 0.1 mol/L HCl/NaOH solutions while the average solar light intensity during that period as recorded using a digital lux-meter was found to be $9.35 * 10^4$ Lx. In a typical experiment, 0.2 – 1.3 g/L of the catalyst were dispersed in several conical flasks containing 50 mL EBT aqueous solution (10–100 ppm) in the presence or absence of scavengers and then immediately transferred under the sunlight for sunlight irradiation (simultaneous combination of adsorption and photocatalysis), this being considered the initial time of the reaction (t = 0). Control experiments under similar conditions without the catalyst were also carried out simultaneously to confirm the photocatalytic nature of the reaction.

3.5 Desorption study and reusability experiments

The desorption study of both pollutants from the mixed metal oxide were done by using 0.5 M NaOH as the desorbing agent. To achieve this, already spent $CoO•CuFe_2O_4$ was eluted in the 0.5M sodium hydroxide solution, washed severally

with deionized water before drying in a conventional oven at 70 °C before reuse. The regenerated $CoO•CuFe_2O_4$ MMO were then used to adsorb/degrade 20 ppm antibiotic/dye solution for six consecutive cycles to establish the reusability potential of the $CoO•CuFe_2O_4$ MMO catalyst.

Chapter 4

RESULTS AND DISCUSSION

4.1 Characterization of Co•Fe LDH and CoO•$CuFe_2O_4$ mixed metal oxide

The typical nitrogen adsorption-desorption isotherm for Co•Fe LDH and CoO•$CuFe_2O_4$ MMO is depicted in Figure 4. As seen from the figure, the Co•Fe LDH and CoO•$CuFe_2O_4$ mixed metal oxide both exhibited type IV isotherm according to the (IUPAC) classification with H_3 hysteresis and large N_2 uptake at p/p_o greater than or equal to 0.85 which is typical of LDH based samples implying a mesoporous size distribution (Di et al., 2017; Huang et al., 2017). It can also be observed from the figure that the N_2 absorbed onto the CoO•$CuFe_2O_4$ mixed metal oxide is higher than that of the LDH. Hence, the CoO•$CuFe_2O_4$ MMO possesses a significantly larger specific surface area (SSA) of 348.5 m^2/g, wider pore size of 5.8 nm and pore volume of 0.715 cm^3/g as compared to the Co•Fe LDH which had 105.3 m^2/g, 3.6 nm and 0.569 cm^3/g respectively. This result is ascribed to removal of interlayer ions and water present in the Co•Fe LDH after the calcination process (Balsamo et al., 2012). The higher SSA and pore volume of the CoO•$CuFe_2O_4$ can provide more active sites and will aid the rapid transport of adsorbate molecules into the interconnected pore structure thereby enhancing the adsorption and photocatalytic capacity of the CoO•$CuFe_2O_4$ mixed metal oxide (Lei et al., 2017).

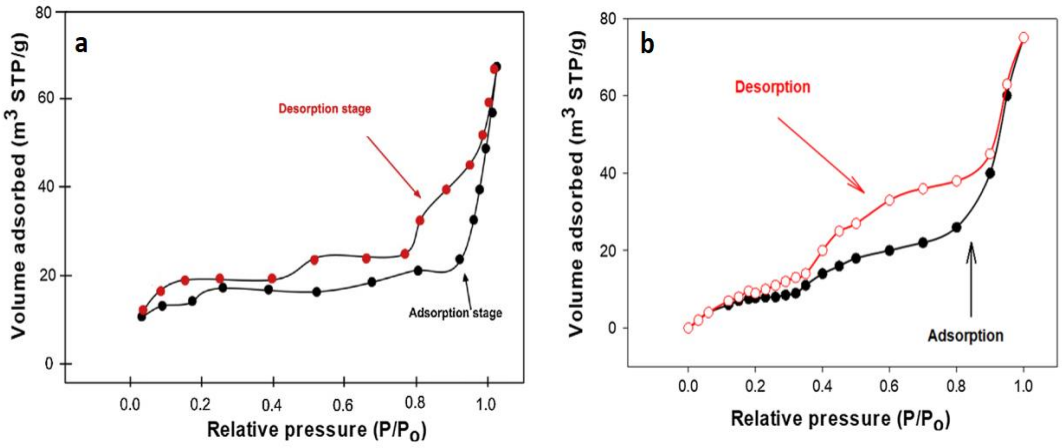

Figure 4: Nitrogen adsorption-desorption isotherm curve of Co•Fe LDH and $CoO•CuFe_2O_4$ mixed metal oxide

The FTIR spectrum of both Co•Fe LDH and $CoO•CuFe_2O_4$ is depicted in Figure 5. Co•Fe LDH exhibited a broad band located at 3500 cm^{-1} which could be attributed to the O-H group from the interlayer water molecules. Sharp peak obtained at 1360 cm^{-1} is assigned to the anti-symmetric stretching mode of the NO_3^- anion present in the Co•Fe LDH (Mahjoubi et al., 2017). However, for the $CoO•CuFe_2O_4$ MMO, there was a decrease in the intensity of the O-H peak due to calcination which also led to the collapse of the layered structure as a result of dehyroxylation. Also the disappearance of the strong band of NO_3^- confirmed that the layered structure of the Co•Fe LDH collapsed and rearranged due to denitration. Finally, adsorption peaks obtained at 643, 579 and 477 cm^{-1} confirms the presence of metal-oxygen-metal vibrations i.e. Co-O, Cu-O and Fe-O in the brucite-type layer of both samples (Chen et al., 2018; Oladipo and Ifebajo 2018).

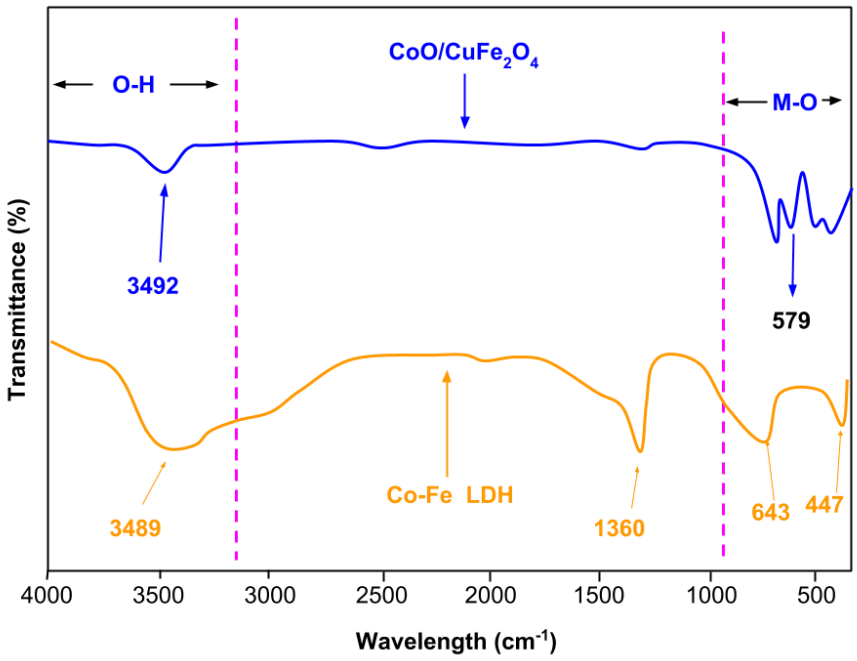

Figure 5: FTIR spectrum of Co•Fe LDH and CoO•$CuFe_2O_4$ MMO

The SEM images of Co•Fe LDH and CoO•$CuFe_2O_4$ is shown in Fig. 6. As seen from the figure, Co•Fe LDH (Fig. 5a) had an irregular, hexagonal interlaced platelet-like morphology with some small cracks visible at the edges of the hexagonal sheets (Ifebajo et al., 2018). This may be due to the rapid conversion of the Iron(III)hydroxide and Co(II)hydroxide particles into hydrotalcites which is consistent with a previous study reported by Rasouli (2017). Also, the compositions of Co and Fe are almost same in all regions except the circled regions. In the case of CoO•$CuFe_2O_4$ MMO obtained after calcination, the surface morphology did not really change at all. This indicates that calcination of the Co•Fe LDH sample did not have a profound effect on the surface morphology of the MMO. However, larger particles can be found on the surface of CoO•$CuFe_2O_4$ implying the growth of the CuO on the surface of the aggregated Fe_3O_4 and CoO particles. Thus, it is expected that the slight changes in the surface morphology of the CoO•$CuFe_2O_4$ MMO may influence its adsorptive and photocatalytic properties.

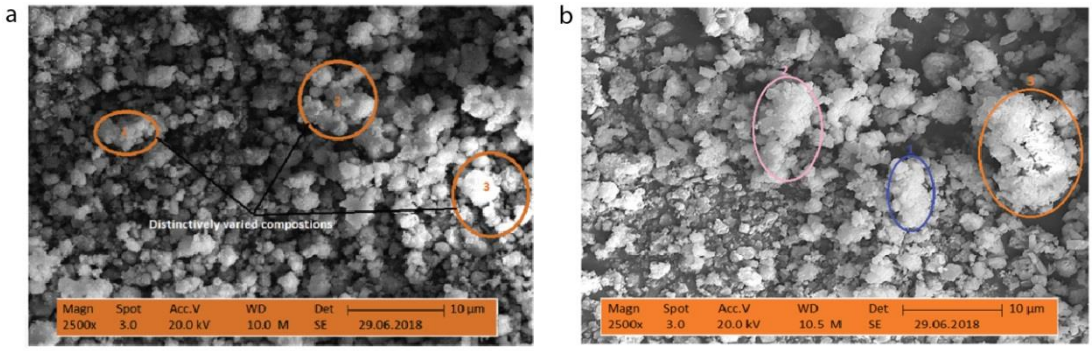

Figure 6: SEM image of (a) Co•Fe LDH and (b) $CoO•CuFe_2O_4$

Crystal structures and energy dispersive X-ray analysis of the synthesized $CoO•CuFe_2O_4$ MMO and Co•Fe LDH is displayed in Fig. 7. The major characteristic diffraction peaks, (003), (006), (101), (012), (400), (531) and (021) observed in the Co•Fe LDH sample (Figure 6a) indicates the nature of nitrate intercalated LDH phase (JCPDS no. 50-0235) (Rasouli et al., 2017). The XRD pattern of $CoO•CuFe_2O_4$ on the other hand showed that the MMO is composed of cubic spinel-structured $CuFe_2O_4$ and face-centered cubic CoO (JCPDS card no. 034-0425). The cobalt(II)oxide displayed characteristic diffraction peaks at 2Θ equal 36.2°, 42.9°,62.6°,74.3° and 78.1° which corresponds to the (111), (200), (220), (311) and (222) lattice plane of cobalt(II)oxide (JCPDS no. 65-2902). $CuFe_2O_4$ reflection planes of (202), (311), (400), (511) and (440) were also obtained in the $CoO•CuFe_2O_4$ MMO.

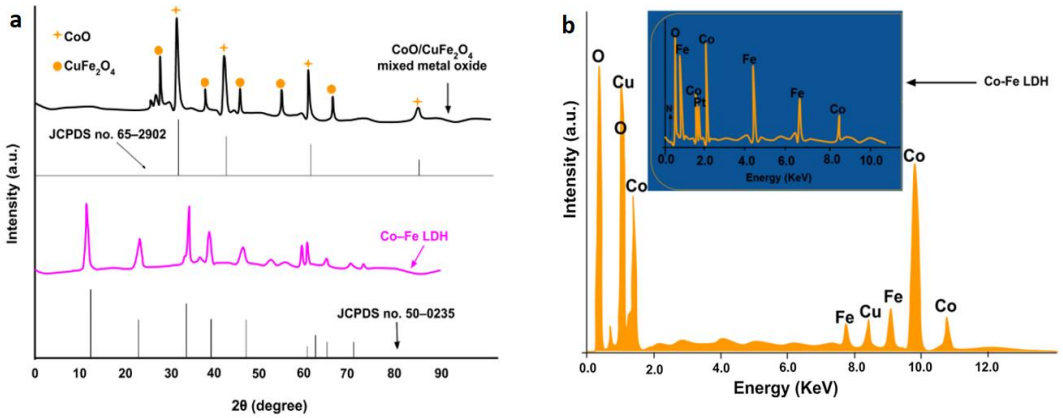

Figure 7: (a) XRD pattern and (b) EDX of Co•Fe LDH and $CoO•CuFe_2O_4$ MMO

Energy-dispersive X-ray mapping and point analyses were applied to determine the elements present in both samples (Figure 7b). The EDX spectrum clearly indicates that the respective metals; copper, cobalt, Iron and oxygen are distributed uniformly and homogeneously within the walls of the $CoO•CuFe_2O_4$ MMO. Copper ions on the other hand was not found in the spectrum of Co•Fe LDH (Fig. 7b insert). Furthermore, the Co/Fe mole ratio was found to reduce from 2.89 in the Co•Fe LDH to 1.96 in the $CoO•CuFe_2O_4$ MMO. Thus, indicated the insertion of copper ions in the layered framework of the Co•Fe LDH. No impurities were detected in any of the peaks. This indicates the phase purity exhibited by both the Co•Fe LDH and $CoO•CuFe_2O_4$ MMO samples investigated.

The TGA thermographs of both samples are presented in Figure 8. TGA curve of Co•Fe LDH exhibited three distinctive weight losses in the temperature range of 50-120 °C, 120-500 °C and 500-950 °C. The first weight loss of ~ 19% observed is due to the loss of physically absorbed and interlayer water present in the Co•Fe LDH. Additional weight loss of about 8% in the second step is attributed to the removal of interlayer nitrate ions and dehydroxylation of the LDH sheets. Finally, a further 8.5

% weight loss is possibly due to the further removal of nitrate ions and the formation of Co•Fe metal oxides from the LDH.

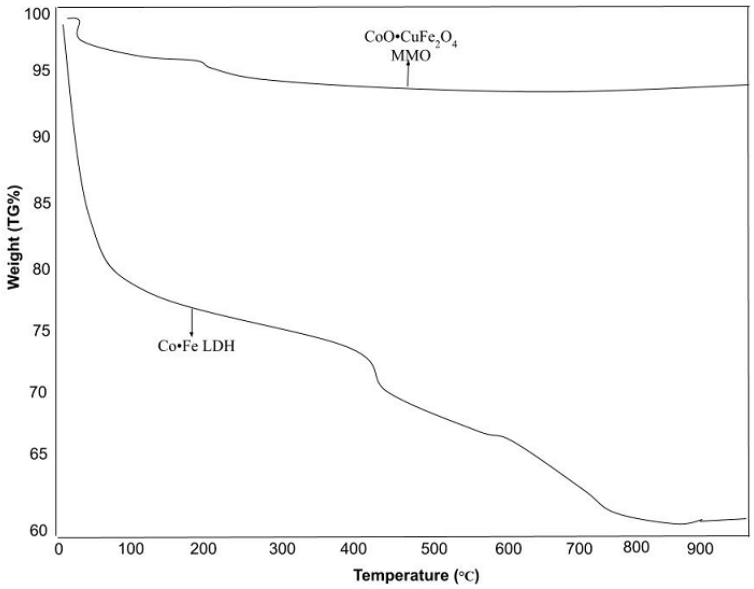

Figure 8: TGA curves for Co•Fe LDH and $CoO•CuFe_2O_4$ mixed metal oxide

The TGA curve of the $CoO•CuFe_2O_4$ MMO on the other hand showed apparent weight losses of about 2.7% at 50-300 °C and 1.2 % at 300-700 °C indicating complete removal of the nitrate ions and formation of $CuFe_2O_4$ spinel specie which was detected in the XRD of $CoO•CuFe_2O_4$ mixed metal oxide. The $CoO•CuFe_2O_4$ mixed metal oxide retained more than 95% of its initial mass after the thermal analysis.

Figure 9 displays the magnetic hysteresis loops and UV-vis diffuse reflectance spectrum of Co•Fe LDH and $CoO•CuFe_2O_4$ at room temperature. The results (Figure 9a) from the magnetic hysteresis loops displayed the ferromagnetic behavior of both samples. Apparently, the partial introduction of Cu^{2+} and calcination of the Co•Fe LDH improved the magnetic properties of the $CoO•CuFe_2O_4$ MMO since the corresponding value of the saturation magnetization, M_s increased from 83.2 emu/g

for the mixed metal oxide to 61.3 emu/g for the LDH. This behavior is consistent with studies reported elsewhere (Oladipo et al., 2019). Hence, the M_s of the CoO•$CuFe_2O_4$ MMO is sufficient for fast separation from any solution by an external magnetic after use.

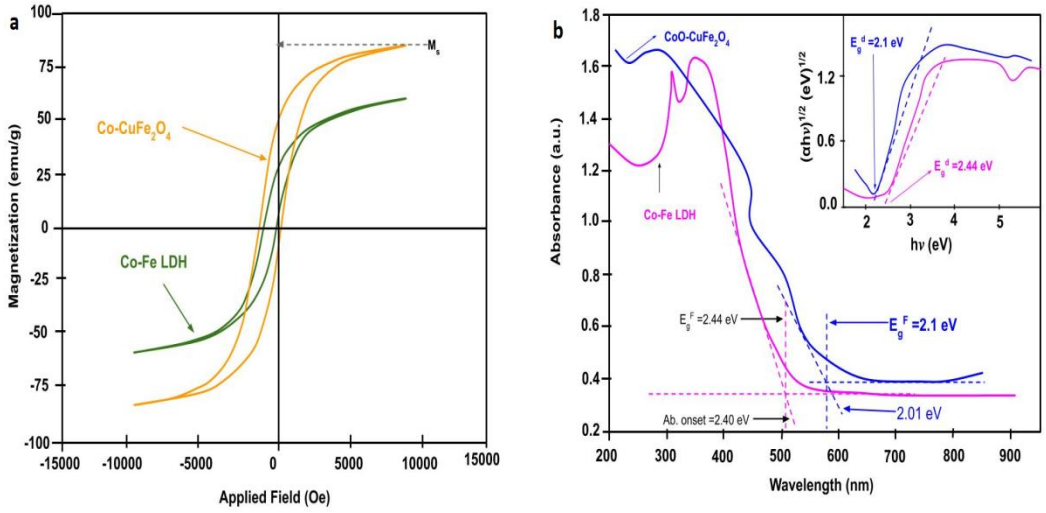

Figure 9: Magnetic hysteresis loops and UV-vis diffuse reflectance spectra for Co•Fe LDH and CoO•$CuFe_2O_4$ mixed metal oxide

As is well known, the optical band gap of any photocatalyst is an important factor that has a significant impact on its photocatalytic applications. To this end, the optical response of the Co•Fe LDH and CoO•$CuFe_2O_4$ MMO was accessed using UV-vis diffuse reflection spectroscopy. The obtained UV-Vis spectrums for both samples were recorded in the range of 200-900 nm and are shown in Figure 9b. It can be seen from the figure that both samples exhibited a broad adsorption in the range studied suggesting that they can absorb light both in the UV and visible region (Oladipo et al., 2019). However, compared to the Co•Fe LDH, the CoO•$CuFe_2O_4$ MMO exhibited a stronger band adsorption and slightly red-shift adsorption in the visible region which was ascribed to the coupling effect of the CoO and $CuFe_2O_4$.

The optical band gap energy was estimated using eq. 7 below for both samples considering the direct adsorption wavelengths of 508 and 590 nm was found to be 2.44 eV for Co•Fe LDH and 2.1 eV for the CoO•$CuFe_2O_4$ respectively.

$$E_g = \frac{1240}{\lambda} \quad (7)$$

Where, E_g represents the optical band gap of the samples and λ is the wavelength of adsorption band.

4.2 Evaluation of adsorption parameters for removal of Tetracycline

4.2.1 Effect of initial TET solution pH

Solution pH is a very important variable to consider when determining optimum conditions for the adsorptive removal of any pollutant via adsorption. To this end, the impact of varying TET solution pH with respect to the removal capacity of the CoO•$CuFe_2O_4$ MMO was carefully investigated with the results obtained depicted in Figure 10 below.

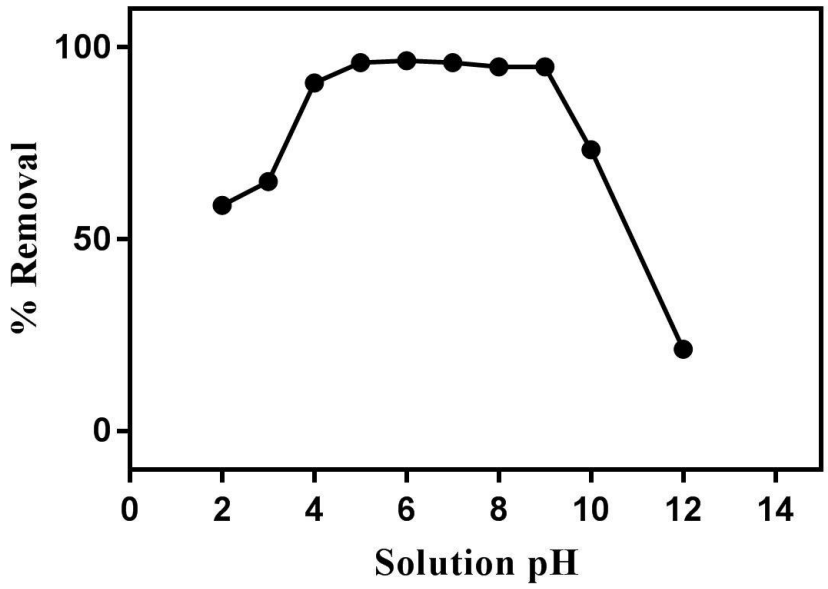

Figure 10: Effect of TET solution pH (C_o= 20 mg/L, T = 298 K)

As revealed in the figure, the tetracycline removal by the mixed metal oxide clearly depends on the solution pH. The removal efficiency $CoO•CuFe_2O_4$ MMO increased steadily from pH 2.0 to 5.0 reaching ~ 96.6% at pH 6.0 before decreasing rapidly from pH 9.0 to 12.0. This observed trend can be attributed both to the pH dependent speciation of TET and the surface chemistry of the $CoO•CuFe_2O_4$ MMO as seen in Figure 11 (Oladipo and Ifebajo, 2018).

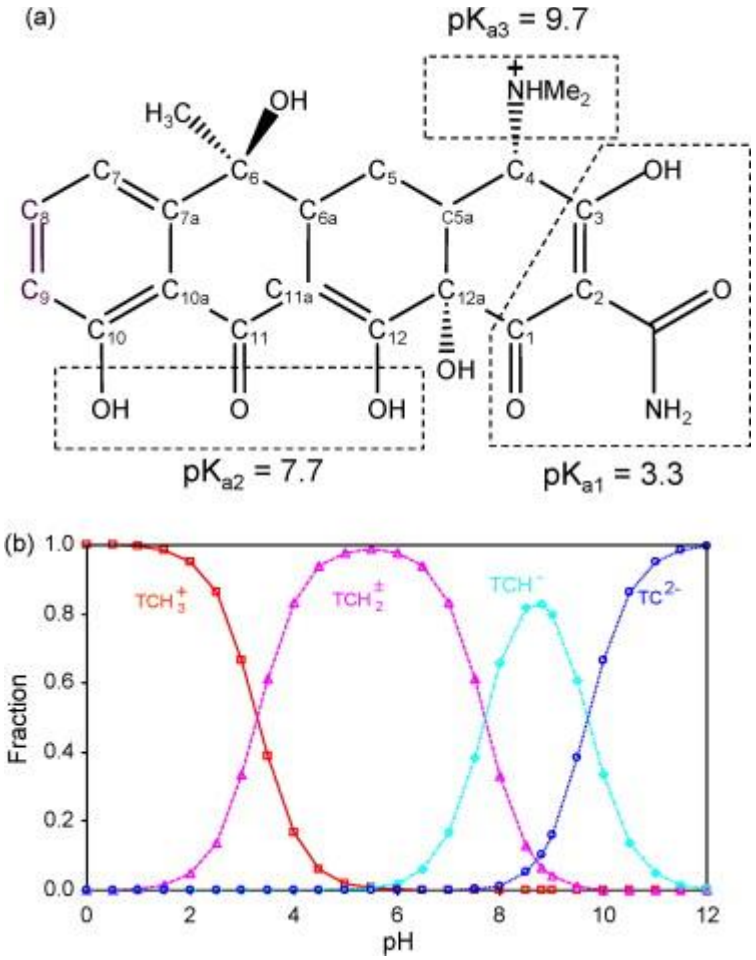

Figure 11: Molecular structure (a) and speciation (b) of TET under different pH
Source: Chang et al., 2009

Minimum adsorptive removal occurred when TET molecules were present in the ionized form both at very acidic pH (where TET exists predominantly in the cationic form at pH value below 3.3) and alkaline pH (anionic form of TET as TCH^- and TC^{2-}

at pH > 9.7) while optimum removal efficiencies were obtained when TET molecules were present in the zwitterion form (pH 3.3 – 7.7) and the $CoO•CuFe_2O_4$ mixed metal oxide was negatively charged (pH > pH_{pzc} 5.8). This proves that the $CoO•CuFe_2O_4$ can perform very well even at neutral pH since there was a 96.1% removal obtained at pH 7.0.

4.2.2 Effect of $CoO•CuFe_2O_4$ dosage

The result of $CoO•CuFe_2O_4$ MMO dosage change (25–100 mg) on the removal efficiencies and equilibrium uptake capacities of TET (initial TET solution pH and concentration of 6.0 and 20 mg/L) is represented in Figure 12. It was observed that the removal efficiency of $CoO•CuFe_2O_4$ increases from 52 % to 92% as the $CoO•CuFe_2O_4$ MMO dosage increases to 50 mg. This is likely due to the availability of more active and vacant sites on the $CoO•CuFe_2O_4$ MMO as the mass of adsorbent increases at constant TET concentration (Chen et al., 2018). A further increase in mass from 50 to 100 mg did not significantly impact the removal efficiency. Thus, the optimum dosage was determined to be 50 mg i.e. 1 g/L of $CoO•CuFe_2O_4$ MMO.

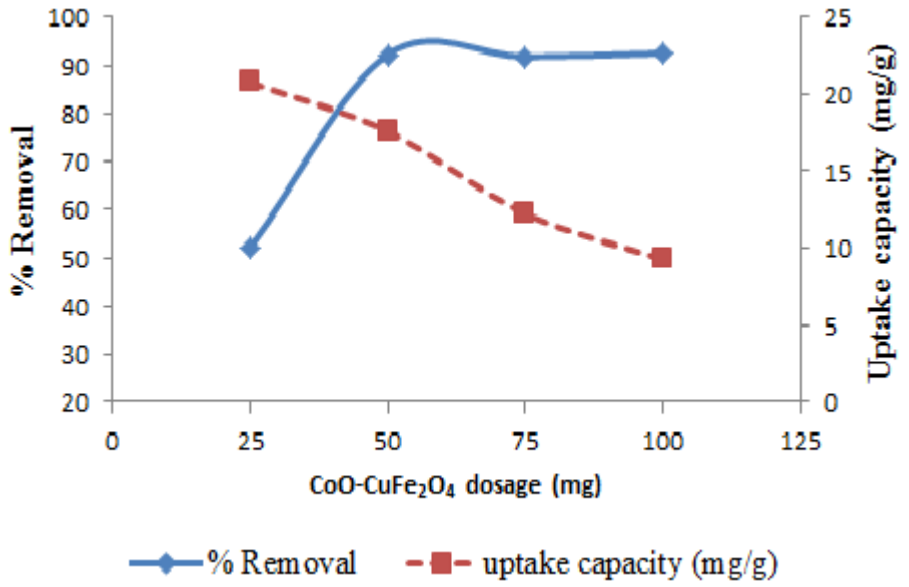

Figure 12: Effect of CoO•$CuFe_2O_4$ dosage on removal efficiency and uptake capacity of TET (Co = 20 mg/L, T = 298 K, pH = 6.0)

However, the equilibrium uptake capacity i.e. amount of TET absorbed by the CoO•$CuFe_2O_4$ MMO decreased steadily from 20.8–9.3 mg/g as CoO•$CuFe_2O_4$ dosage increases. This is likely due to the agglomeration or overlap of adsorption sites of CoO•$CuFe_2O_4$ MMO available for TET adsorption as the quantity of the MMO increases which effectively reduces the total effective surface and thereby increases the diffusion path length of the TET molecules. Also, this aggregation might make some of the TET molecules attached loosely to CoO•$CuFe_2O_4$ surface via reversible bonds to be readily desorbed from the surface of the CoO•$CuFe_2O_4$ MMO adsorbent (Marzbali et al., 2016).

4.2.3 Effect of adsorption contact time and TET concentration

The uptake capacity of CoO•$CuFe_2O_4$ mixed metal oxide with respect to contact time was determined by changing the initial TET concentration from 40–100 mg/L at 298 K (Figure 13). It can be observed clearly from the figure that the amount of TET absorbed onto the CoO•$CuFe_2O_4$ mixed metal oxide increases (from 36.05–74.10 mg/g) as TET concentration increased. This is largely because an increase in

adsorbate i.e. TET concentration led to a corresponding increase in the solution's driving force required to overcome all mass transfer resistances between the solution-solid phase and this subsequently enhanced the rate of adsorptive removal of TET (Liu et al., 2012). At higher TET concentration, more TET molecules is expected to diffuse faster from the $CoO•CuFe_2O_4$ surface into its micropores. Quite notably, the adsorptive removal of the TET molecules occurred rapidly in the first 60 min for all adsorption tests carried out. Apparently, a further extension in the adsorption contact time did not have a drastic impact on the uptake capacity of the $CoO•CuFe_2O_4$ MMO adsorbent.

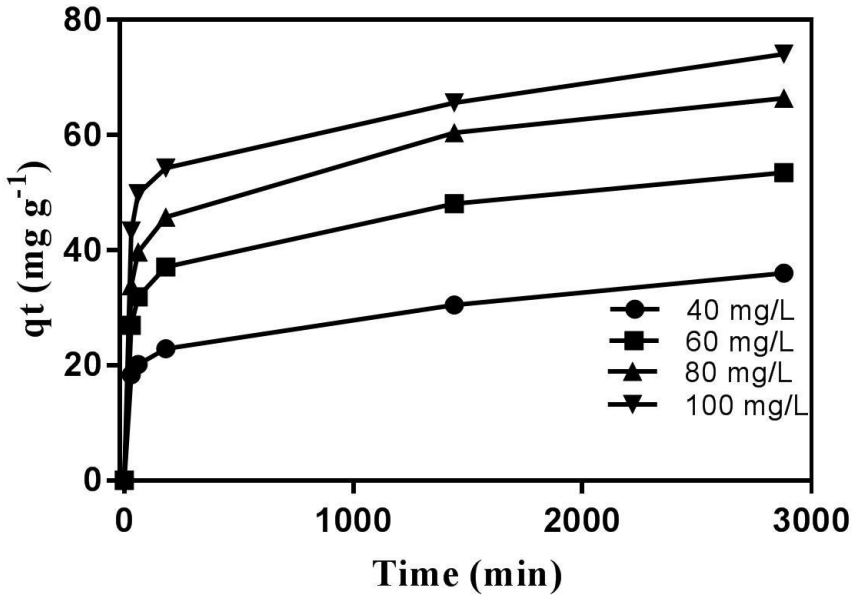

Figure 13: Effect of initial TET concentration and contact time on uptake capacities of $CoO•CuFe_2O_4$ (pH = 6.0, $CoO•CuFe_2O_4$ mass = 50 mg, T = 298 K)

The initial rapid rate of adsorption observed at the start of the adsorption process for all TET concentrations was due to the availability of abundant negatively charged vacant sites on $CoO•CuFe_2O_4$ MMO surface at pH 6.0. Also, at higher TET concentrations, the amount of TET molecules available for adsorption relative to the

surface area of $CoO•CuFe_2O_4$ MMO is high and this resulted in the higher uptake capacity exhibited by the adsorbent as initial concentration increased (El Haddad et al., 2013). Finally, as seen from the figure, the rate of adsorption slowed down considerably after 180 minutes due to the slow diffusion of the TET molecules into the pores of the $CoO•CuFe_2O_4$ MMO (Chen et al., 2010).

4.2.4 Effect of counter ions on TET adsorption

The presence of salts and co-existing pollutants such as heavy metals, dyes etc. in industrial waste water often causes an increase in ionic strength and this in turn could influence the ability of any adsorbent to effectively remove the desired pollutant from the system due to the interaction between pollutant, co-existing pollutants and adsorption sites on an adsorbent surface (Oladipo and Gazi, 2014). In this study, we determined the influence of counter ions (Cl^- and NO_3^-) at different concentrations (0–4 g L^{-1}) on the removal efficiency of the $CoO•CuFe_2O_4$ mixed metal oxide. Results obtained are depicted in Figure 14.

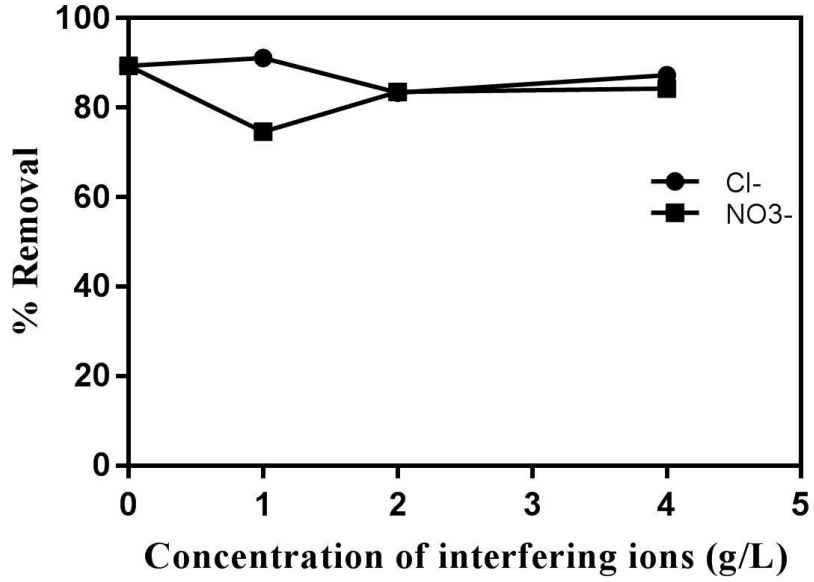

Figure 14: Effect of counter ions on removal on removal efficiency of TET by $CoO•CuFe_2O_4$ (pH = 6.0, $CoO•CuFe_2O_4$ mass = 50 mg, T = 298 K)

Fig. 14 shows that both counter ions did not have a significant impact on the percentage removal of $CoO•CuFe_2O_4$ MMO as the quantity of TET absorbed slightly decreased slightly from ~ 89.4 % (removal efficiency without any counter ions) to 87.3% and 84.3% as the concentration of NaCl and KNO_3 increased to 4 g L^{-1}. The slight decrease in removal efficiency might be because the counter ions slightly competed with TET molecules for identical active sites on $CoO•CuFe_2O_4$ mixed metal oxide.

4.2.5 Effect of TET solution Temperature

As shown in Figure 15, the effect of varying TET solution temperature on the removal efficiency of TET was examined in the range of 25-50 °C. It was found that the removal efficiency of $CoO•CuFe_2O_4$ mixed metal oxide increased from 74.1% to 87.2% with an increase in reaction temperature which simply implies that the adsorptive removal process of TET must be endothermic. This result was attributed to a combination of the reduced TET solution viscosity and the expansion of active sites on $CoO•CuFe_2O_4$ as temperature increases, which in turn facilitates an increase in the rate of the molecular TET diffusion molecules from the external boundary layer into the pores of $CoO•CuFe_2O_4$ MMO. Similar reports were obtained by other researchers for removal of TET using AC derived from tomato (*Lycopersicon esculentum* Mill) and apricot nut shells (Saygılı and Güzel 2016; Marzbali et al., 2016).

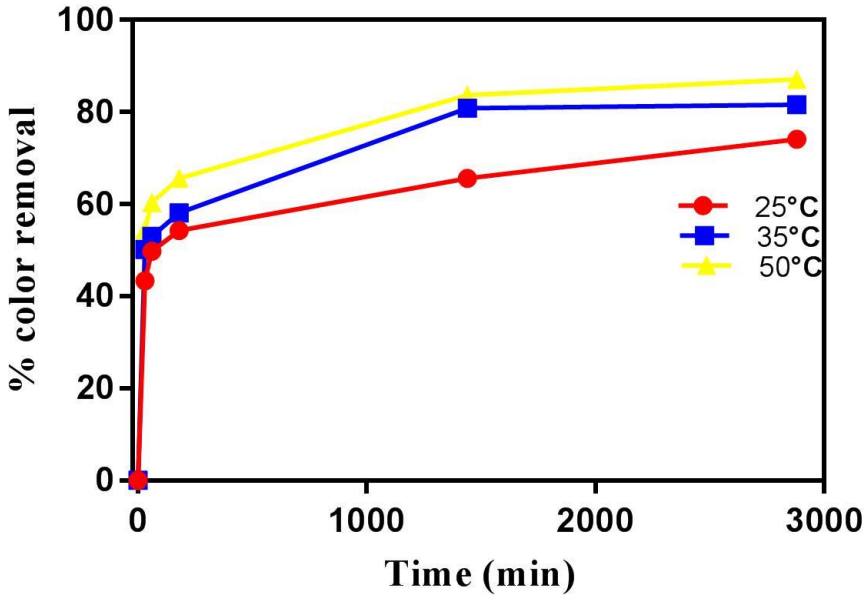

Figure 15: Effect of TET solution Temperature on removal efficiency of TET by $CoO•CuFe_2O_4$ (pH = 6.0, $CoO•CuFe_2O_4$ mass = 50 mg, Co = 100 mg/L)

4.2.6 Comparison of performance of $CoO•CuFe_2O_4$ for TET removal

The maximum adsorption capacity q_{max} of TET removal reported in this study was compared with previous reports for TET removal by various adsorbents under varying operating conditions and tabulated in Table 4. It can be easily concluded that the $CoO•CuFe_2O_4$ mixed metal oxide showed a reasonably good adsorption capacity for TET and can serve as an alternative adsorbent for TET removal in WWTPs.

Table 4: Comparison of adsorptive performance of $CoO•CuFe_2O_4$ for EBT removal with other reported studies

Adsorbent	pH	Temp (K)	Co (mg L^{-1})	q_m (mg g^{-1})	Reference
$CoO•CuFe_2O_4$	6.0	298	200	175.4	This study
$NH_2Fe_3O_4/CuSiW_{12}NP$	6.80	299 ± 2	250	191.86	Ou et al., 2016
MCBB	-	298	100	63.3	Oladipo et al., 2017
Non activated SBA Activated SBA	6.0	318	150	15.23 87.87	Yang et al., 2016
PP,PS and *Sc* biocomposites	6.0	-	150	12.27-18.35	Ersan 2016
Palygorskite	8.7	-	800	99	Chang et al., 2009

- : not given, MCBB: magnetic chicken bone-based biochar, SBA: sludge based adsorbent, PP: polypropylene, PS: polystyrene, *Sc*: *Saccharomyces cerevisiae yeast*

4.3 Adsorption study and Sunlight assisted degradation of EBT

The photocatalytic degradation of EBT at varying experimental conditions (pH, contact time, dosage and concentration with and without scavengers) was studied under direct sunlight irradiation to determine the catalytic efficacy of $CoO•CuFe_2O_4$ and ascertain optimum experimental conditions.

4.3.1 Effect of EBT initial solution pH

Pollutant initial solution pH has a vital role to play in the degradation process because changes in solution pH can lead to a corresponding change or alter the surface properties of any heterogeneous photocatalyst. To investigate this effect i.e. pH on the photocatalytic potential of $CoO•CuFe_2O_4$, set of experiments were conducted under same experimental conditions by varying the EBT solution pH from 2.0–10.0. Fig 16 shows that the EBT solution pH played a very important role in the removal process of EBT dye molecules as the degradation efficiency reduced from ~ 99% to 70 % as initial EBT solution pH increased from 2.0 to 4.0 for 20 ppm EBT solution. It is also worthy to note that there was no significant EBT removal at pH

7.0 and 10.0. This trend can be explained based on the chemistry of EBT dye and the surface activity of the photocatalyst $CoO•CuFe_2O_4$ MMO. As determined earlier, the pH_{pzc} of the photocatalyst was found to be 5.8 while the zeta potential of EBT is negative from pH 2.0 to 12.0 (Ifebajo et al., 2018). Therefore, at pH greater than 5.8, the $CoO•CuFe_2O_4$ MMO surface becomes negatively charged and this led to an electrostatic repulsion between the dye containing negative sulfonate groups and the catalyst, hence the low removal observed at pH 7 and 10. However, lowering the pH of the dye solution led to a strong interface between the anionic azo dye and the positively charged $CoO•CuFe_2O_4$ surface via electrostatic attraction which in turn led to higher photocatalytic efficiency (Lee et al., 2015).

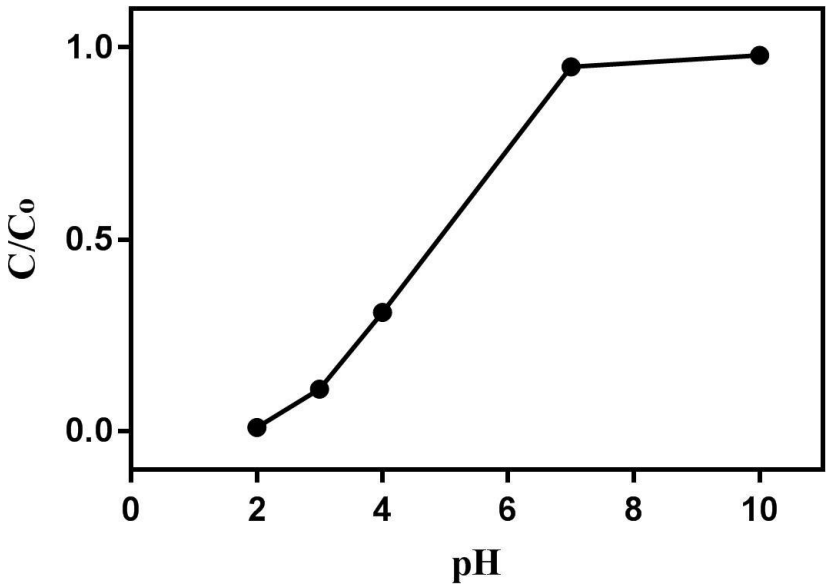

Figure 16: Effect of EBT initial solution pH on removal of EBT dye

4.3.2 Effect of degradation reaction contact time and $CoO•CuFe_2O_4$ dosage

Figure 17 shows the impact of varying $CoO•CuFe_2O_4$ MMO dosage on the degradation efficiency of EBT dye. As observed from the figure, the direct photolysis of EBT dye molecules without the $CoO•CuFe_2O_4$ MMO catalyst only had

a slight impact on the removal of EBT from aqueous phase with this value considered in all calculations related to the dye photodegradation. However, upon exposure to direct sunlight in the presence of the $CoO•CuFe_2O_4$ MMO catalyst, the photodegradation efficiency increased from 45% to 92% as $CoO•CuFe_2O_4$ MMO catalyst dosage increased from 0.2 – 1.0 g/L. Additionally, a further increase in the catalyst dosage to 1.3 g/L did not have a significant impact on the oxidation efficiency of the catalyst after 90 min. This observed trend in the decolorization rate is ascribed to the increase in the total number of active sites available on $CoO•CuFe_2O_4$ MMO as the surface area of the metal oxide catalyst increases which in turn led to increase in the amount of photogenerated electron-hole pair and a corresponding increase in the number of radicals produced (Oladipo, 2018; Kaur et al., 2015). Our optimum dosage was found to be 50 mg (1.0 g/L) as a further increase in $CoO•CuFe_2O_4$ MMO catalyst dosage only had a minimal effect on the rate of EBT degradation.

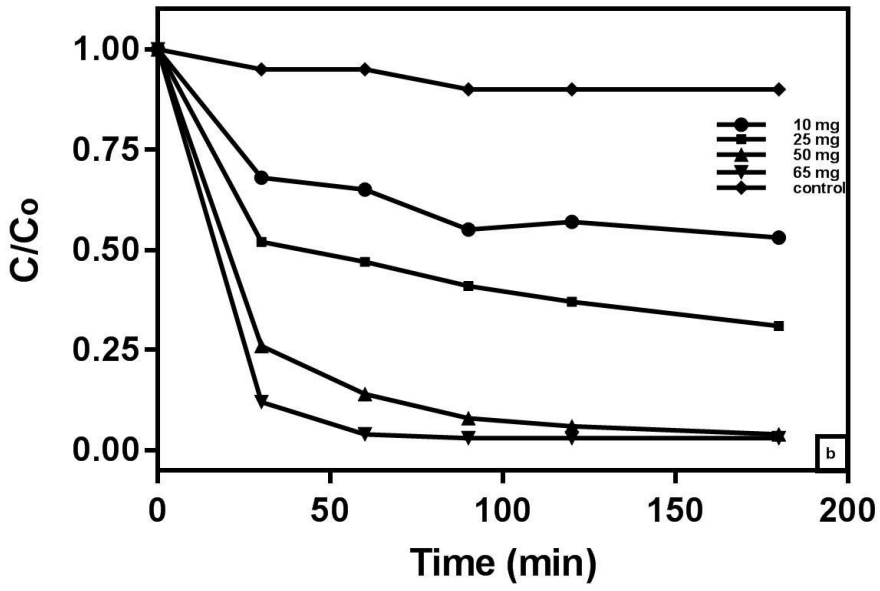

Figure 17: Effect of degradation reaction contact time and $CoO•CuFe_2O_4$ dosage on removal of EBT dye

4.3.3 Effect of degradation reaction contact time and EBT concentration

Fig. 18 shows the influence of change in EBT concentration (10-100 ppm) at constant amount of $CoO•CuFe_2O_4$ catalyst (50 mg) with respect to reaction contact time (180 min). As is evident from the Figure, the rate of decolorization reduces from 96% to 60% as dye concentration increases. This might be due to either one of or both reasons discussed next.

Firstly, as EBT initial concentration increased, more EBT molecules are absorbed on the $CoO•CuFe_2O_4$ catalyst surface thereby requiring more active sites on the catalyst for efficient degradation. However, as both sunlight intensity and catalyst dosage are constant, the photogenerated radicals produced on the surface of the catalyst will not change but remain constant irrespective of EBT dye concentration. Hence, the generated radicals will be insufficient to decolorize the EBT molecules leading to reduced decolorization efficiency of the catalyst.

Also, increasing the EBT dye concentration will reduce the amount of photons that arrive on the surface of the photocatalyst since more light is absorbed by dye molecules thereby inhibiting the excitation of the $CoO•CuFe_2O_4$ photocatalyst and its potential to form electron hole pairs which are responsible for degradation (Pouretedal et al., 2005). These two factors might have led to the decrease in degradation efficiency of EBT dye as concentration increased.

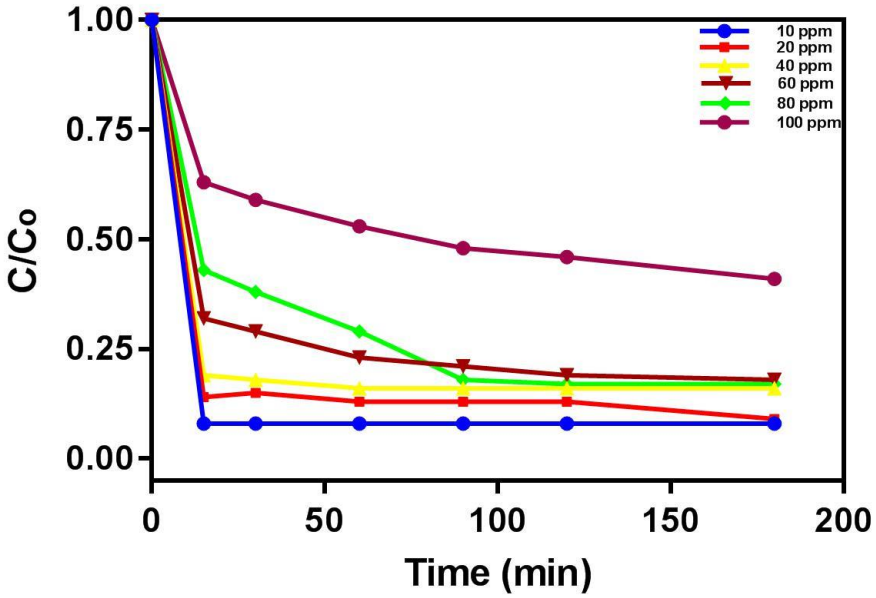

Figure 18: Effect of degradation reaction contact time and EBT initial concentration on removal of EBT dye

4.3.4 Effect of radical scavengers and proposed mechanism for EBTdegradation

It is well known in the photocatalytic degradation process that reactive species RS such as; holes (h^+), superoxide ($^{\bullet}O_2^-$) and hydroxyl radicals ($^{\bullet}OH$) are responsible for photocatalytic reactions. In order to determine the contribution of each RS on the photodegradation of EBT dye, three chemical reagents; t-butyl alcohol (*t*-BuOH), benzoquinone (BQ) and ammonium oxalate (AO) were selected as radical scavengers for the hydroxyl, superoxide radicals and h^+. As displayed in Figure 19, there was a dramatic drop in the photocatalytic efficiency of ~ 62% and 69.3% as the concentration of AO increased from 5 to 10 mM within 180 min of reaction. A possible reason for this is that at low pH values, photogenerated h^+ act as the predominant oxidizing species whereas at neutral or alkaline pH, $^{\bullet}OH$ radicals are responsible for oxidizing the organic pollutant (Lee et. al., 2015). Hence, this resulted in the observed suppression of the photoactivity of the CoO•$CuFe_2O_4$ MMO catalyst since AO acts as an electron donor or h^+ trap. In addition, the EBT removal

was only slightly suppressed in the presence of both *t*-BuOH (5.5 and 5.7%) and BQ (3.1%) indicating that mostly the h^+ played a significant role in the photodegradation process.

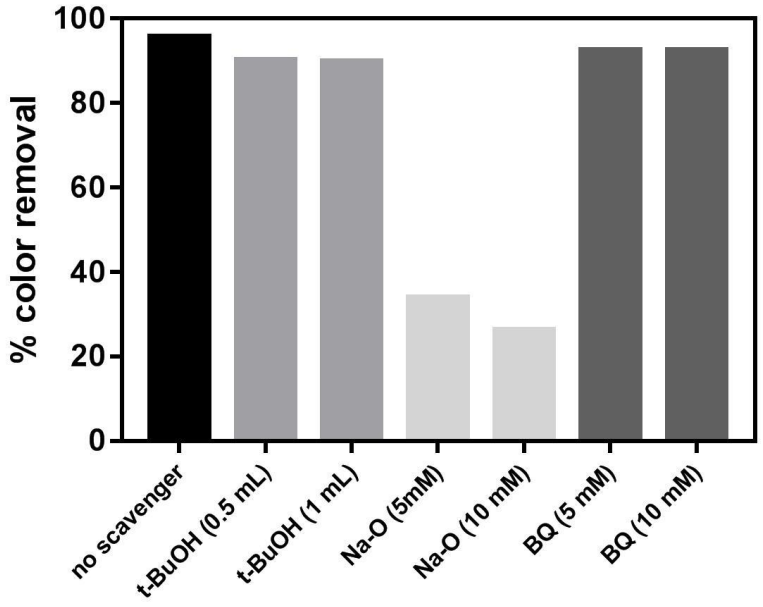

Figure 19: Effect of radical scavengers on removal of EBT dye

The probable mechanism (Figure 20) for the sunlight assisted degradation of EBT using the mixed metal oxide photocatalyst can be speculated from the experimental results obtained in the first part of this section (effect of scavengers) and the Uv-Vis analysis. $CoO•CuFe_2O_4$ MMO was excited under solar irradiation to generate the electron-hole pair whereby electrons are promoted from the valence band (VB) to the conduction band (CB) leaving similar number of holes in the VB as seen in the scheme and eq. 8. Upon generating the electron-hole pair, a series of chemical reactions (eq. 9-13) take place on the surface of the $CoO•CuFe_2O_4$ MMO catalyst which eventually leads to the production of the reactive species RS responsible for degrading the molecules of EBT dye.

Electrons generated in the CB react with dissolved oxygen present in the system to form the superoxide radical ($^{\bullet}O_2^-$) while $OH^{\bullet}$ radicals are produced from the reaction of h^+ with the absorbed water on the surface of the $CoO{\bullet}CuFe_2O_4$ MMO photocatalyst (eq. 9 and 10). Both reactions occurring in eq. 9 and 10 prevent the rapid recombination of the sunlight photogenerated electrons and holes that are produced in the first step. Further reactions (eq. 11–13) also occur simultaneously to generate more hydroxyl radicals as shown below.

$$CoO{\bullet}CuFe_2O_4\ MMO + \text{sunlight } (h\nu) \rightarrow e^-_{cb} + h^+_{vb} \quad (8)$$

$$h^+_{vb} + H_2O \rightarrow OH^{\bullet} + H^+ \quad (9)$$

$$e^-_{cb} + O_2 \rightarrow {}^{\bullet}O_2^- \quad (10)$$

$${}^{\bullet}O_2^- + H^+ \rightarrow HO_2^{\bullet} \quad (11)$$

$$HO_2^{\bullet} + HO_2^{\bullet} \rightarrow H_2O_2 + O_2 \quad (12)$$

$$H_2O_2 \rightarrow 2OH^{\bullet} \quad (13)$$

$$(h^+_{vb}, {}^{\bullet}O_2^-, OH^{\bullet}) + EBT \rightarrow CO_2 + H_2O + \text{other intermediates} \quad (14)$$

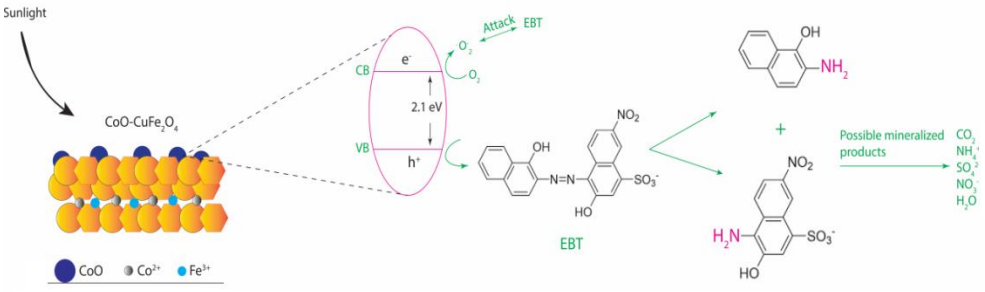

Figure 20: Schematic illustration for the proposed mechanism of EBT degradation under solar irradiation using $CoO{\bullet}CuFe_2O_4$ MMO

The results show that the positive h^+ generated (eq. 8) was the dominant RS that subsequently oxidized the EBT molecules via a direct oxidative pathway while the $OH^{\bullet}$ radicals and superoxide anion also had a role to play in decomposing the dye (eq. 14).

4.3.5 Combination of adsorption and photocatalysis and adsorption study

To investigate the role of adsorption in the sun light assisted degradation of EBT using $CoO•CuFe_2O_4$ MMO, a known amount of the photocatalyst was added to varying dye concentrations (20–100 ppm) and stirred on a mechanical shaker in the laboratory for 60 min during the day to establish the adsorption and desorption equilibrium on the surface of the photocatalyst before sunlight irradiation, this being considered the initial time of the reaction (t = 0). Results obtained from the three reaction conditions i.e. adsorption (A), direct photocatalysis without adsorption (P) and adsorption followed by photocatalysis (A-P) for 20 and 40 ppm EBT initial concentration is shown in Fig. 21.

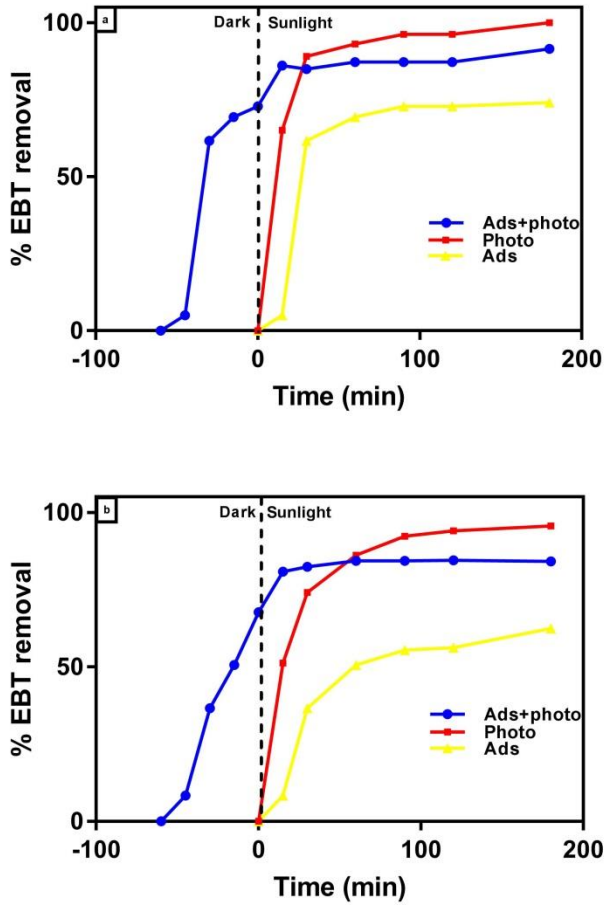

Figure 21: Comparison of adsorption, direct photocatalysis and combination of adsorption and photocatalysis on degradation of EBT at different concentrations (a) 20 ppm (b) 40 ppm

During adsorption followed by photocatalysis (A-P), 91% and 84% removal was observed for EBT concentrations after 240 min reaction time (60 min adsorption and 180 min sunlight irradiation) as compared to ~96% and 92% removal obtained by simultaneous adsorption and photocatalysis (P) using the $CoO•CuFe_2O_4$ MMO photocatalyst after 90 min. The slight decrease observed in the degradation efficiency of A-P was possibly due to the dye already absorbed on the catalyst surface which when on exposure to sunlight acted as a filter reducing the photoactive volume, thereby leading to lower production of the RS needed for the photocatalytic process. However, in the case of direct photocatalysis without adsorption (P), the dye

molecules were simultaneously absorbed and degraded on the $CoO•CuFe_2O_4$ MMO surface of the catalyst except at very high EBT concentrations (60 and 100 ppm) where the dye molecules might hinder the solar light intensity reaching the catalyst surface. It can also be seen from the graphs that the $CoO•CuFe_2O_4$ MMO can also serve as a good adsorbent for the removal of EBT dye.

After a comparison of all three reaction conditions, the direct photocatalysis (P) was found to be the most efficient and effective process for the removal of EBT from aqueous phase since it took less time and still exhibited higher or similar color removal to the A-P and adsorption process. Similar observations were reported elsewhere for the photocatalytic mineralization and degradation of ampicillin and oxytetracycline by graphene sand composite and chitosan supported BiOCl (Priya et al., 2016).

To further understand the combined effect of adsorption with photocatalysis A-P, the Langmuir-Hinshelwood model (Eq. (15)) was applied to study the kinetics of EBT degradation under sunlight irradiation.

$$-In\left(\frac{C_t}{C_i}\right) = k_{app}\, t \tag{15}$$

Where;

C_i and C_t represent the initial EBT concentrations before irradiation and EBT concentrations at time *t* during irradiation and K_{app} is the apparent P.F.O degradation rate constant.

Linearity of the all plots obtained (not shown) with high R^2 values ranging from 0.96–0.99 suggests that the photocatalytic degradation follows P.F.O kinetic model

in both cases (Table 5). However, the simultaneous combination of adsorption and photocatalysis P had higher K_{app} at all concentrations studied showing that the removal process is more efficient when combined together. In fact, for low concentrations (20 and 40 ppm), the K_{app} is more than twice that of the A-P process. Also, increasing the EBT dye concentration from 20–100 ppm led to a subsequent decrease in the degradation rate constant in both cases.

Table 5: Apparent P.F.O kinetic rate constant and R^2 values of $CoO•CuFe_2O_4$

EBT conc (ppm)	Photocatalysis (P)	Ads+photocatalysis (A-P)
20	K_{app} = 0.017 1/min R^2 = 0.9896	K_{app} = 0.0395 1/min R^2 = 0.98
40	K_{app} =0.013 1/min R^2 = 0.9732	K_{app} = 0.0312 1/min R^2 = 0.9759
60	K_{app} =0.012 1/min R^2 =0.963	K_{app} = 0.014 1/min R^2 = 0.9854
100	K_{app} =0.0081 1/min R^2 = 0.9801	K_{app} = 0.0084 1/min R^2 = 0.9939

4.3.6 Comparison of photocatalytic performance of $CoO•CuFe_2O_4$ for EBT removal

The performance of the catalyst for removal of EBT in this study was compared with other previous reports and presented in Table 6. The as-synthesized $CoO•CuFe_2O_4$ MMO relatively outperformed most reported catalysts and is also more economical to use since solar irradiation (i.e. sunlight) required for its operation is free. Thus said, it can be inferred that the $CoO•CuFe_2O_4$ MMO catalyst can be used for photocatalytic applications especially in waste water remediation.

Table 6: Comparison of photocatalytic performance of $CoO•CuFe_2O_4$ for EBT removal with other reported studies

Photocatalyst	Reaction conditions					% Removal	Ref
	pH	C_o	Time (min)	Dosage (g L-1)	Light source		
$CoO•CuFe_2O_4$	2	40 ppm	90	1.0	Sunlight	A-P:84.5, P: 92.3	This work
N-doped TiO_2 coated on glass spheres	-	5 mg L^{-1}	210	0.4	visible (Λ = 400-800 nm), UV light (Λ =365 – 400)	Vis:31 UV: 41	Vaiano et al., 2015
Gd_2CoMnO_6	-	5 ppm	90	1.0	Hg lamp	89	Mohassel et al., 2018
NiS-P zeolite	9.1	20 ppm	180	0.8	Hg lamp	78.5	Ejhieh, & Khorsandi 2010
ZnO	3	0.08 mM	60	1.0	UV light	83	Kaur & Singhal 2015
$Nd_2Zr_2O_7$	-	-	50	-	UV light	84	Zinatloo-Ajabshir & Salavati-Niasari (2017)
SWCNT/ Nd,N,S-TiO_2						89.2	
MWCNT /Nd,N,S-TiO_2		20 ppm	240	1.0	Xenon lamp solar simulator	85.8	Mamba et al., 2015
TiO_2		25 mg L^{-1}	90	0.25	UV light	82	Kansal et al., 2013
$Nd_2Sn_2O_7$	-	-	70	-	Osram lamp (Λ = 400-700 nm)	94.6	Zinatloo-Ajabshir et al., 2018

- : not mentioned

4.4 Adsorption Isotherms and Kinetics

4.4.1 Isotherm studies for TET and EBT

Adsorption isotherm studies offer valuable insights on how the adsorbent, $CoO•CuFe_2O_4$ MMO will bind and interact with both adsorbate molecules i.e. TET and EBT during the adsorption process. These isotherm models can further help to understand the possible mechanism(s) of adsorption and also give a good idea of the adsorptive capacities of the $CoO•CuFe_2O_4$ MMO under the studied conditions.

For this present work, four two-parameter adsorption isotherms related to the adsorption equilibrium studies were tested and fitted to the experimentally obtained adsorption equilibrium data. Figure 22 and 23 display the corresponding linear plots while Table 7 summarizes the corresponding fitted parameters obtained from each isotherm models for the removal of both pollutants by $CoO•CuFe_2O_4$ mixed metal oxide at 298 K.

The applicability of each isotherm equation to ascertain the degree of fitness to the experimental values was determined using the correlation coefficient (R^2) value and two error functions; the Chi-square test χ^2 and normalized standard deviation Δq_e (eq. 16 and 17). The model that best fits the experimental data should have the lowest error values and highest correlation coefficient when compared with other models.

$$\chi 2 = \sum \frac{(q_{e,exp} - q_{e,cal})^2}{q_{e,cal}} \quad (16)$$

$$\Delta q_t = \sqrt{\sum (\frac{[\frac{q_{e,exp} - q_{e,cal}}{q_{e,exp}}]^2}{(N-1)}} \quad (17)$$

Where; $q_{e,exp}$ and $q_{e,cal}$ represent the experimentally obtained and calculated adsorption capacity of $CoO•CuFe_2O_4$ MMO and N represent the amount of observations/data points in the experimentally obtained data.

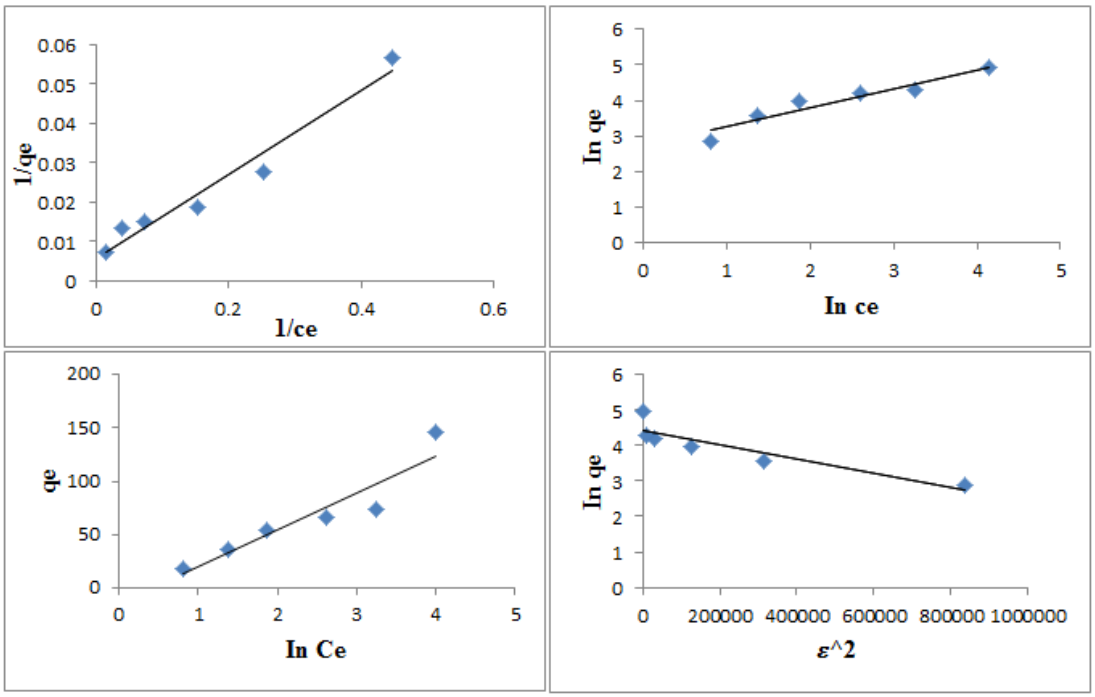

Figure 22: Langmuir, Freundlich, Temkin and Dubinin- Radushkevich isotherm plots for TET

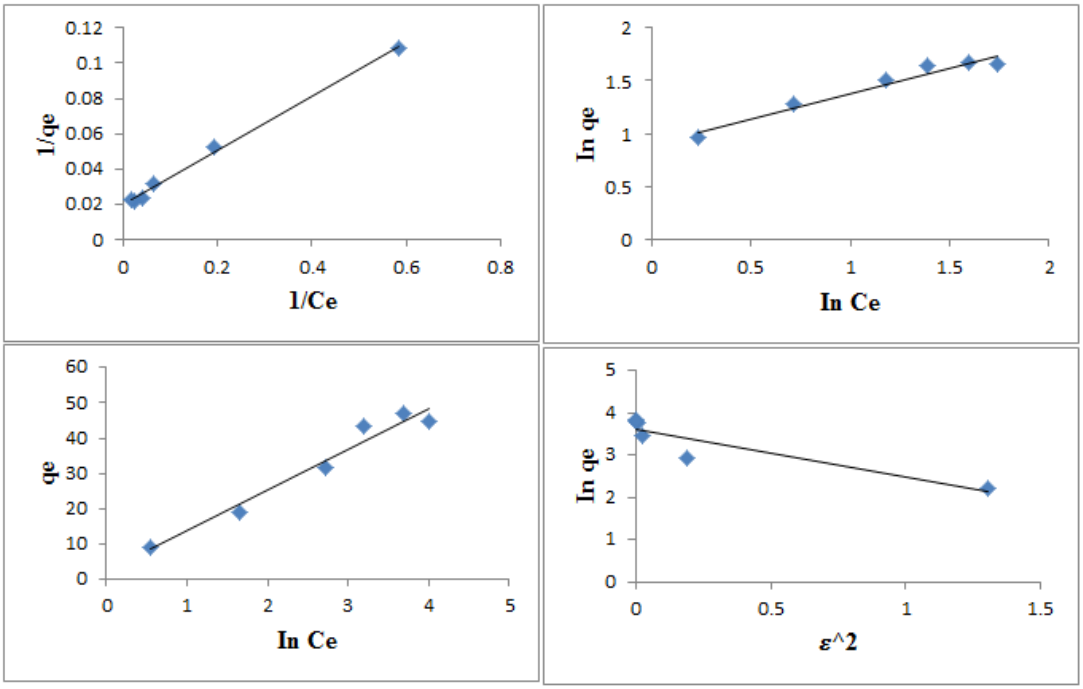

Figure 23: Langmuir, Freundlich, Temkin and Dubinin- Radushkevich isotherm plots for EBT

A thorough comparison of the R^2 values determined for all isotherm models in Table 2 shows that the Langmuir isotherm gives a reasonable fit for the removal of both pollutants by CoO•$CuFe_2O_4$ with the R^2 values closer to 1 when compared to the other isotherms evaluated. Also, according to the error values obtained, the Langmuir model had the lowest error values. Therefore, the adsorption of both pollutants by the CoO•$CuFe_2O_4$ mixed metal oxide takes place via a monolayer adsorption of both pollutants on the CoO•$CuFe_2O_4$ MMO adsorbent homogeneous surface.

Table 7: Adsorption isotherm parameters of TET and EBT onto $CoO•CuFe_2O_4$ at 298K

Isotherms	Linear plots	TET Parameters	EBT parameters
Langmuir	$\frac{1}{q_e} vs. \frac{1}{C_e}$	R^2 = 0.9593 q_{max} = 175.4 mg/g K_L = 0.053 L/mg χ^2 = 3.44 Δq_e = 0.22 R_L = 0.09 – 0.485	R^2 = 0.9955 q_{max} = 51.8 mg/g K_L = 0.125 L/mg χ^2 = 0.99 Δq_e = 0.15 R_L = 0.07 - 0.44
Freundlich	$In\ q_e\ vs.\ In\ C_e$	R^2 = 0.9231 K_F = 15.02 L mg^{-1} *1/n* = 0.541 χ^2 = 5.50 Δq_e = 0.32	R^2 = 0.958 K_F = 8.02 L mg^{-1} *1/n* = 0.479 χ^2 = 3.16 Δq_e = 0.29
Temkin	$q_e\ vs.\ In\ C_e$	R^2 = 0.8786 B = 34.815 A = 0.648 L g^{-1} b = 71.2 J mol^{-1} χ^2 = 7.25 Δq_e = 0.32	R^2 = 0.9648 B = 11.559 A = 1.203 L g^{-1} b = 214.3 J mol^{-1} χ^2 = 1.18 Δq_e = 0.21
Dubinin- Radushkevich (D-R)	$In\ q_e\ vs.\ \varepsilon^2$	R^2 = 0.8421 β = 2.001 mol^2/KJ^2 q_{max} = 82.20 mg g^{-1} E = 0.500 KJ mol^{-1} χ^2 = 53.03 Δq_e = 0.525	R^2 = 0.8338 β = 1.137 mol^2/KJ^2 q_{max} = 37.79 mg g^{-1} E = 0.663 KJ mol^{-1} χ^2 = 9.57 Δq_e = 0.59

The Langmuir and Freundlich isotherm constants i.e. K_L and *1/n* are important parameters that are essential in predicting the nature of the adsorption process i.e. if it adsorption is termed favorable or not.

A key characteristic obtained from the Langmuir isotherm is a dimensionless equilibrium constant (R_L) called the separation factor which indicates the shape of the isotherm and whether the adsorption process can be considered favorable or not (Anandkumar and Mandal, 2011).

$$R_L = \frac{1}{(1+K_L C_O)} \quad (18)$$

If R_L values are greater than unity (i.e. $R_L > 1$), process is unfavorable, linear if $R_L = 1$, irreversible if $R_L = 0$ and favorable if R_L values lie between 0 and 1 ($0 < R_L < 1$).

All R_L values obtained in our study for both pollutants lie between 0 and 1 at 298 K and confirmed that the removal of both pollutants by $CoO•CuFe_2O_4$ is favorable under this condition studied.

The Freundlich isotherm constant *1/n* can also be used to predict the adsorption process. If *1/n* values lie between 0 and 1 (0< *1/n* <1), this signifies a favorable adsorption process. *1/n* equal to 1 (*1/n* = 1) assumes adsorption is homogeneous with no interaction between adsorbates while *1/n* values above 1 (*1/n* > 1) identifies the process to be unfavorable (Chieng et al., 2015). Quite similar to the results we obtained from the Langmuir analysis, the adsorption of both TET and EBT was also found to be favorable since the values of *1/n* for both pollutants were less than 1 i.e. 0.541 for TET and 0.479 for EBT respectively.

Furthermore, mean sorption energy (*E)* calculated from the D-R isotherm model can give valuable information regarding the nature of adsorption and adsorption mechanism as follows (Sayğılı and Güzel, 2016):

- *E* : 8 –16 kJ/mol is regarded as chemisorption
- *E*: < 8 KJ/mol is indicative of physical adsorption

As shown in Table 5, the magnitudes of *E* in both cases were < 8 KJ/mol which is indicative of a physical adsorption process.

4.4.2 Kinetic studies for TET and EBT

Four widely used kinetic models (Table 3) were used in this study to test the experimentally obtained data and predict the adsorption mechanism involved in the adsorptive removal of both TET and EBT. The linearized forms of all equations and linear plots obtained are presented in Table 8 and Figures 24 and 25 respectively,

while all kinetic parameters, error functions and correlation coefficients R^2 for both TET and EBT 40 mg/L initial concentration also summarized in Table 8.

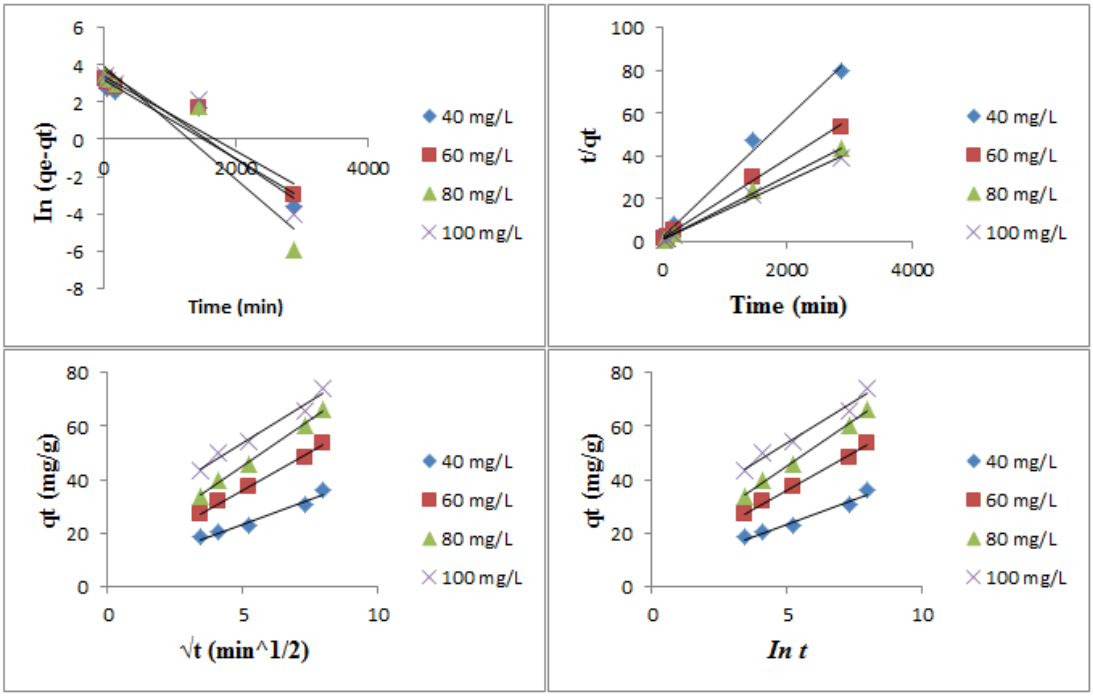

Figure 24: First-order, second-order, intraparticle and Elovich plot for TET

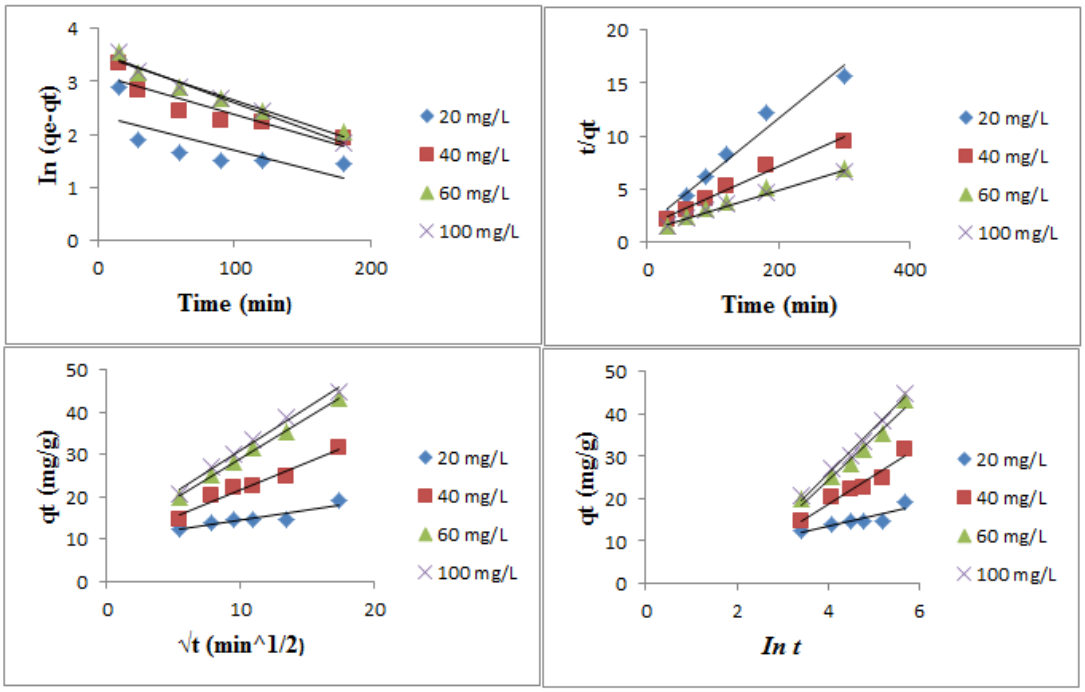

Figure 25: First-order, second-order, intraparticle and Elovich plot for EBT dye

As depicted in the table below, R^2 value(s) for the P.F.O model (0.9797 & 0.9336) is slightly lower than that of P.S.O model (0.993 & 0.9735) for both TET and EBT. In addition, the errors functions for P.F.O are higher than the P.S.O model. This result clearly indicates that the P.F.O model cannot be the valid model to explain the adsorption process of TET and EBT on the $CoO•CuFe_2O_4$ adsorbent. As evident from the table, the P.S.O model displayed a higher correlation coefficient R^2 and lower error values when compared to the P.F.O model. Moreover, q_e values calculated from the P.S.O were closely fitted to the experimental data when compared to that obtained from the P.F.O. It should also be noted that the P.F.O correlation coefficient R^2 for all concentrations of both pollutants studied were found in the range of (0.2114-0.9808) which were far lower than that obtained by the PSO kinetic model (0.9735-0.999). This suggests that the removal of both pollutants by $CoO•CuFe_2O_4$ followed the P.S.O kinetic model, indicating the process is possibly controlled by valence forces and/or chemisorption (Yang et al., 2016).

In the case of TET, although the P.S.O kinetic model had a slightly higher correlation coefficient R^2 (0.993) when compared to the Elovich model (0.969), however its error functions are higher than that obtained by the Elovich model. This indicates that the Elovich model also fitted the experimental results reasonably well. Hence, we concluded that the adsorptive removal of TET molecules probably occurs by a combination of chemisorption, ion-exchange reactions and surface reconstruction mechanism (Oladipo et al. 2016).

The initial kinetics sorption rate; h (mg/g min) can also be determined from the P.S.O kinetic model using eq. 19 below;

$$h = K_2 {q_e}^2 \quad (19)$$

Where, K_2 and q_e are the P.S.O rate constant and calculated adsorption capacity of CoO•$CuFe_2O_4$. As seen in the table, the initial rate of sorption for EBT is slightly higher than that of TET meaning a faster initial rate of adsorption occurred in EBT when compared to TET.

Table 8: kinetic parameters of TET and EBT onto CoO•$CuFe_2O_4$ at 298K

Kinetics	Linear kinetic plots	TET Parameters Co (40 mg/L)	EBT parameters Co (40 mg/L)
Pseudo-first order P.F.O	$In\ (q_e - q_t)\ \ vs.\ \ k_1 t$	R^2 = 0.9797 K_{FO} = 0. 0008 min^{-1} $q_{e\ (exp)}$ = 36.05 mg g^{-1} $q_{e\ (cal)}$ = 16.59 mg g^{-1} χ^2 = 15.62 Δq_t = 1.81	R^2 = 0.9366 K_{FO} = 0.0103 min^{-1} $q_{e\ (exp)}$ = 32.78 mg g^{-1} $q_{e\ (cal)}$ = 27.58 mg g^{-1} χ^2 = 15.26 Δq_t = 0.67
Pseudo-second order P.S.O	$\frac{t}{q_t}\ \ vs.\ \ t$	R^2 = 0.993 K_{SO} = 0.00036 g mg^{-1} min^{-1} $q_{e\ (exp)}$ = 36.05 mg g^{-1} $q_{e\ (cal)}$ = 36.10 mg g^{-1} h = 0.405 mg/g min χ^2 = 8.61 Δq_t = 0.41	R^2 = 0.9735 K_{SO} = 0.0005 g mg^{-1} min^{-1} $q_{e\ (exp)}$ = 32.78 mg g^{-1} $q_{e\ (cal)}$ = 35.8 mg g^{-1} h = 0.643mg/g min χ^2 = 0.97 Δq_t = 0.21
Intra-particle diffusion	$q_t\ \ vs.\ \ t^{0.5}$	R^2 = 0.9928 K_{IP} = 0.350 mg/g min C = 17.32 g/mg	R^2 = 0.8536 K_{IP} = 1.783 mg/g min C = 2.555 g/mg
Elovich	q_t *vs. In t*	R^2 = 0. 9693 α = 4.915 mg/g min β = 3.705 g/mg χ^2 = 0.24 Δq_t = 0.09	R^2 = 0.9447 α = 8.36 mg/g min β = 6.736 g/mg χ^2 = 43.43 Δq_t = 2.09

The adsorption of any adsorbate by an adsorbent is characterized by several stages that involves the transfer of adsorbate/solute molecules from solution phase onto the adsorbent i.e. CoO•$CuFe_2O_4$ surface via external or film diffusion, before its eventual gradual intraparticle diffusion into the internal pores of the CoO•$CuFe_2O_4$ adsorbent,

This process is slow and is usually regarded as the rate-governing step. The three kinetics models discussed above cannot identify the possible diffusion mechanism of both EBT and TET; therefore the intraparticle diffusion model formulated by Weber and Morris (1963) was tested using the kinetic adsorption results.

According to this theory, the quantity of adsorbate molecules adsorbed i.e. q_t (mg/g) varies proportionally with the square root of contact time, i.e. $t^{0.5}$. Therefore, for intraparticle diffusion to be taken as the rate-controlling step, a plot of q_t against $t^{0.5}$ should not only be linear but must pass through the origin (i.e. zero intercept, $C = 0$), otherwise other mechanisms along with intraparticle diffusion are involved. The obtained plot of q_t (mg/g) for both pollutants (initial concentration: 40 mg/L) adsorbed with respect to $t^{0.5}$ is also depicted in Figure 22 and 23 above.

It can be observed that the plots for both TET and EBT were multi-linear i.e. not linear over time and most certainly did not go through the origin of the plots. This proves that intraparticle diffusion was not the only rate-controlling step for both pollutants and other mechanisms maybe involved due to the multi linearity and deviation of these plots from the origin (Ersan, 2016).

4.5 Adsorption thermodynamics of TET removal by $CoO•CuFe_2O_4$

Thermodynamic studies of the adsorption process of TET by $CoO•CuFe_2O_4$ MMO were undertaken in this section to identify if the adsorption process was spontaneous or not. To achieve this, the experimental data obtained by varying temperatures (298.15–323.15 K) were used in calculating thermodynamic parameters; entropy (ΔS°), enthalpy change (ΔH°) and Gibbs free energy change (ΔG°) from the Van't Hoff's equation shown below.

$$\ln K_c = -\frac{\Delta H^\circ}{RT} + \frac{\Delta S^\circ}{R} \quad (20)$$

Where,

R; universal gas constant = 8.314 J mol^{-1} k^{-1}

K_c is the distribution coefficient and *T* in Kelvin (*K*) is the absolute solution temperature of TET.

The distribution coefficient and ΔG° can be calculated using the relations expressed below; eq. (21) and (22).

$$K_c = {}^{C_d}/_{C_e} \quad (21)$$

$$\Delta G^\circ = -RT \ln K_c \quad (22)$$

Where, C_d is the equilibrium amount of TET adsorbed by the CoO•$CuFe_2O_4$ MMO (mg L^{-1}) and C_e also in mg L^{-1} represents the equilibrium concentration of TET remaining in solution phase after adsorption. Figure 26 shows the Van't Hoff's plot for removal of TET.

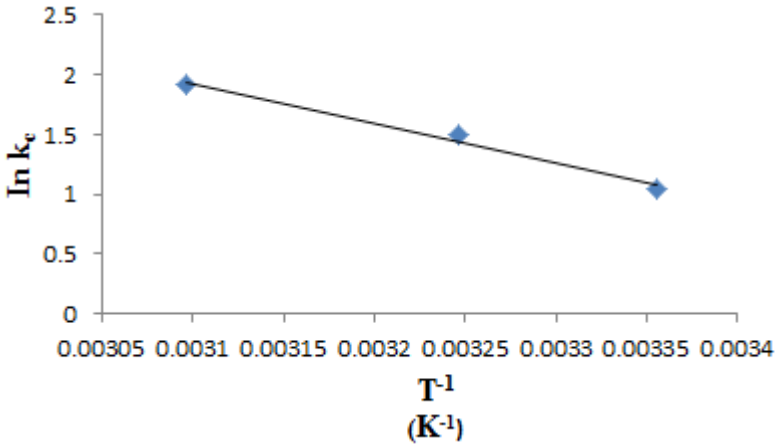

Figure 26: *ln Kc vs 1/T*

As seen from the Figure, the plot of *In* K_c with respect to 1/*T* yielded a straight line. Thermodynamic parameters; Δ*S*° and Δ*H*° displayed in Table 9 were then obtained

from the intercept and slope. As tabulated, both Δ*S*° and Δ*H*° values are positive both indicating the increased randomness observed at the CoO•$CuFe_2O_4$ MMO solid-TET solution interface and the endothermic nature of TET adsorption. The data also presented in the table revealed the thermodynamic feasibility and spontaneous nature of the TET adsorption process due to negative Δ*G*° values which increased (from -2.60 – -5.14 kJ/mol) on increase in adsorption reaction temperature from 298.15–323.15 *K*.

To further support the result showing the impact of changing temperature on sorption of TET, the initial sorption rate, *h* calculated using equation 19 increased steadily from 1.243 to 2.167 mg/g min with increasing temperature. This further confirms that the adsorptive removal process becomes more rapid and spontaneous as temperature increased.

Table 9: Thermodynamic parameters of TET removal by CoO•$CuFe_2O_4$ MMO

Ci (mg/L)	Temp (K)	ΔS° (J/mol K)	ΔH° (KJ/mol)	ΔG° (KJ/mol)	R^2
100	293.15	100.85	27.35	-2.60	0.9886
100	308.15			-3.82	
100	323.15			-5.14	

Finally, the Arrhenius equation expressed below (eq. 23) was applied to determine the activation energy E_a, for the adsorptive removal of TET by the CoO•$CuFe_2O_4$ MMO.

$$\ln K_{SO} = \ln A - \frac{E_a}{RT} \quad (23)$$

Where;

K_{SO} is the P.S.O rate constant (g/ mg min), *A* is the Arrhenius factor and E_a (kJ/mol) represent activation energy.

E_a obtained from the slope of the Arrhenius plot can then be used to determine the nature of the adsorption mechanism/process. When E_a is from 40–800 kJ mol^{-1}, it suggests chemisorption while E_a values between 5 and 40 KJ mol^{-1} are characteristic of physical adsorption (Rani et al., 2015).

From the Arrhenius plot in our study (Figure not shown), E_a was determined to be 6.47 kJ mol^{-1}. This suggested that adsorption of TET by $CoO•CuFe_2O_4$ is a physical process and there was an energy barrier present in the sorption process (Tang et al., 2012). Interestingly, this result also agrees with *E*-value (mean energy of adsorption) previously calculated using the Dubinin- Radushkevich isotherm model.

4.6 Regeneration and reusability of $CoO•CuFe_2O_4$

In practice, it is necessary to evaluate the efficiency and performance of an adsorbent/photocatalyst i.e. $CoO•CuFe_2O_4$ after recycling. Therefore, the performance of the $CoO•CuFe_2O_4$ mixed metal oxide after elution in NaOH, oven-drying at 70 °C before being reapplied for both pollutants was examined and reported in Figure 27. In the case of TET, the removal efficiency did not change at all after 6 cycles (~ 92.3-93.5%) while that of EBT showed only a slight decrease from ~ 100% to 80%.

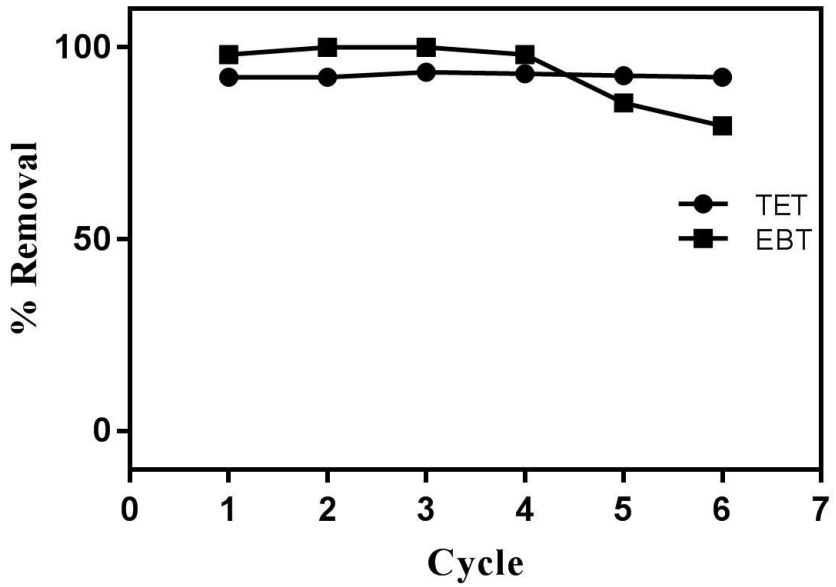

Figure 27: Removal efficiency of $CoO•CuFe_2O_4$ MMO for TET and EBT after 6 cycles (T = 298 K, C_o = 20 mg/L)

As shown in the figure, the degradation efficiency of the photocatalyst for EBT remained stable after 4 cycles although slight decrease in efficiency obtained after 5 cycles might be due to the weakening of the dye adsorption capacity of the catalyst since the active sites present on the $CoO•CuFe_2O_4$ MMO surface might be blocked by already absorbed EBT molecules.

Therefore, it can be concluded that the $CoO•CuFe_2O_4$ mixed metal oxide exhibits good adsorption and catalytic properties and can be reused severally without significant loss in its adsorptive/photocatalytic properties giving it a great potential for practical wastewater treatment facilities.

Chapter 5

CONCLUSION

In this research work, $CoO•CuFe_2O_4$ MMO was successfully synthesized from its corresponding Co•Fe LDH using a simple co-precipitation method and high temperature calcination (500 °C) under inert conditions for 5 hours. The as-synthesized $CoO•CuFe_2O_4$ MMO was characterized and applied as an adsorbent and heterogeneous photocatalyst for the eradication of tetracycline and Eriochrome black T from wastewater effluents under laboratory condition(s). The final conclusions drawn from a thorough analysis of all experimental results are given below:

- Detailed characterization revealed that the $CoO•CuFe_2O_4$ MMO had good magnetic and optical properties with a higher specific surface area in contrast to the Co•Fe LDH.
- The removal and degradation efficiency of $CoO•CuFe_2O_4$ mixed metal oxide was influenced by operational parameters including adsorbent/catalyst dosage, counter ions, pollutant solution pH, contact time.
- Adsorption and photocatalysis trend showed that initial TET and EBT solution pH had a vital role to play in the rapid uptake of both pollutants. Maximum removal for TET and EBT was found to be pH 6.0 and 2.0 respectively.
- The $CoO•CuFe_2O_4$ mixed metal oxide exhibited rapid adsorption kinetics in the first 1h of reaction time and the presence of counter ions/increase in ionic

strength of solution did not really affect the removal efficiency of TET by the adsorbent.

- The experimental data obtained from the removal of both TET and EBT was tested using four kinetic models. The P.S.O kinetic model exhibited the best-fit since it had the lowest error functions and highest R^2 values. Kinetic data also suggests that the diffusion mechanism of both pollutants was rather complex and intraparticle diffusion might be involved in the process but was not the overall rate-determining step with other processes contributing in the sorption process.
- Thermodynamic adsorption studies of TET indicated that removal process was endothermic due to positive ΔH° values and also spontaneous under studied conditions. Activated energy obtained by the Arrhenius plot confirmed the adsorption of TET by $CoO•CuFe_2O_4$ MMO to be a physical process.
- From all isotherm models investigated, the Langmuir isotherm clearly fitted the experimentally obtained equilibrium results based on the error functions ($\chi 2$: 3.43 and 0.99 and Δq_e: 0.22 and 0.14) and correlation coefficient R^2 (0.9592 and 0.9955) values obtained for TET and EBT. This implies a monolayer adsorption on the homogeneous surface of the $CoO•CuFe_2O_4$ MMO. The maximum sorption capacity for TET and EBT was determined as 175.4 and 51.8 mg g^{-1} respectively. This result compares well with other adsorbents reported in literature.
- Simultaneous adsorption and photocatalysis were the most efficient process and showed higher EBT degradation rate. Photogenerated holes h^+ were the dominant reaction specie in the degradation of EBT dye.

- More importantly the $CoO•CuFe_2O_4$ MMO adsorbent/catalyst can be easily separated from wastewater with an external magnet and regenerated with basic elution without any significant impact on its adsorptive capacity after 5-6 regeneration cycles.
- The synthesized $CoO•CuFe_2O_4$ MMO showed promising potential as a heterogeneous catalyst and adsorbent in the remediation of EBT and TET.

In conclusion, these results obtained within the framework of this thesis clearly indicate that the synthesized $CoO•CuFe_2O_4$ MMO can serve as an alternative adsorbent/photocatalyst for the eradication of both tetracycline and Eriochrome Black T from wastewaters. However, more studies are required to determine its full potential as a convenient material for use in industrial and real life applications.

REFERENCES

Akhtar, J., Amin, N. A. S., & Shahzad, K. (2016). A review on removal of pharmaceuticals from water by adsorption. *Desalination and Water Treatment*, *57*(27), 12842-12860.

Aksu, Z. (2005). Application of biosorption for the removal of organic pollutants: a review. *Process biochemistry*, *40*(3-4), 997-1026.

Altın, O., Özbelge, H. Ö., & Doğu, T. (1998). Use of general purpose adsorption isotherms for heavy metal–clay mineral interactions. *Journal of colloid and interface science*, *198*(1), 130-140.

Álvarez-Torrellas, S., Ribeiro, R. S., Gomes, H. T., Ovejero, G., & García, J. (2016). Removal of antibiotic compounds by adsorption using glycerol-based carbon materials. *Chemical Engineering Journal*, *296*, 277-288.

Anandkumar, J., & Mandal, B. (2011). Adsorption of chromium (VI) and Rhodamine B by surface modified tannery waste: Kinetic, mechanistic and thermodynamic studies. *Journal of Hazardous Materials*, *186*(2-3), 1088-1096.

Asad, S., Amoozegar, M. A., Pourbabaee, A., Sarbolouki, M. N., & Dastgheib, S. M. M. (2007). Decolorization of textile azo dyes by newly isolated halophilic and halotolerant bacteria. *Bioresource technology*, *98*(11), 2082-2088.

Baccar, R., Blánquez, P., Bouzid, J., Feki, M., & Sarrà, M. (2010). Equilibrium, thermodynamic and kinetic studies on adsorption of commercial dye by activated carbon derived from olive-waste cakes. *Chemical Engineering Journal*, *165*(2), 457-464.

Bajpai, S. K., Bajpai, M., & Rai, N. (2012). Sorptive removal of ciprofloxacin hydrochloride from simulated wastewater using sawdust: Kinetic study and effect of pH. *Water SA*, *38*(5), 673-682.

Balsamo, N., Mendieta, S., Oliva, M., Eimer, G., & Crivello, M. (2012). Synthesis and characterization of metal mixed oxides from Layered Double Hydroxides. *Procedia Materials Science*, *1*, 506-513.

Barka, N., Ouzaouit, K., Abdennouri, M., & El Makhfouk, M. (2013). Dried prickly pear cactus (Opuntia ficus indica) cladodes as a low-cost and eco-friendly biosorbent for dyes removal from aqueous solutions. *Journal of the Taiwan Institute of Chemical Engineers*, *44*(1), 52-60.

Ben-Ali, S., Jaouali, I., Souissi-Najar, S., & Ouederni, A. (2017). Characterization and adsorption capacity of raw pomegranate peel biosorbent for copper removal. *Journal of Cleaner Production*, *142*, 3809-3821.

Bui, X. T., Vo, T. P. T., Ngo, H. H., Guo, W. S. & Nguyen, T. T. 2016 Multicriteria assessment of advanced treatment technologies for micropollutants removal at large-scale applications. *Science of the Total Environment*, **563**, 1050-1067.

Cape Town water crisis: Residents urged to turn off toilet taps. Accessed online on August 10, 2019 from https://www.bbc.com/news/world-africa-42836560

Carbone, M., Briancesco, R., & Bonadonna, L. (2017). Antimicrobial power of Cu/Zn mixed oxide nanoparticles to Escherichia coli. *Environmental Nanotechnology, Monitoring & Management*, *7*, 97-102.

Chang, P. H., Li, Z., Yu, T. L., Munkhbayer, S., Kuo, T. H., Hung, Y. C., ... & Lin, K. H. (2009). Sorptive removal of tetracycline from water by palygorskite. *Journal of Hazardous Materials*, *165*(1-3), 148-155.

Chen, S., Zhang, J., Zhang, C., Yue, Q., Li, Y., & Li, C. (2010). Equilibrium and kinetic studies of methyl orange and methyl violet adsorption on activated carbon derived from Phragmites australis. *Desalination*, *252*(1-3), 149-156.

Chen, W., Xing, J., Lu, Z., Wang, J., Yu, S., Yao, W. & Wang, S. (2018). Citrate-modified Mg–Al layered double hydroxides for efficient removal of lead from water. *Environmental chemistry letters*, *16*(2), 561-567.

Chieng, H. I., Lim, L. B., & Priyantha, N. (2015). Sorption characteristics of peat from Brunei Darussalam for the removal of rhodamine B dye from aqueous solution: adsorption isotherms, thermodynamics, kinetics and regeneration studies. *Desalination and Water Treatment*, *55*(3), 664-677.

Dąbrowski, A. (2001). Adsorption—from theory to practice. *Advances in colloid and interface science*, *93*(1-3), 135-224.

Deng, L., Shi, Z., Peng, X., & Zhou, S. (2016). Magnetic calcinated cobalt ferrite/magnesium aluminum hydrotalcite composite for enhanced adsorption of methyl orange. *Journal of Alloys and Compounds*, *688*, 101-112.

Di, G., Zhu, Z., Zhang, H., Zhu, J., Lu, H., Zhang, W., ... & Küppers, S. (2017). Simultaneous removal of several pharmaceuticals and arsenic on Zn-Fe mixed metal oxides: Combination of photocatalysis and adsorption. *Chemical Engineering Journal*, *328*, 141-151.

El Haddad, M., Slimani, R., Mamouni, R., Laamari, M. R., Rafqah, S., & Lazar, S. (2013). Evaluation of potential capability of calcined bones on the biosorption removal efficiency of safranin as cationic dye from aqueous solutions. *Journal of the Taiwan Institute of Chemical Engineers*, *44*(1), 13-18.

Erşan, M. (2016). Removal of tetracycline using new biocomposites from aqueous solutions. *Desalination and Water Treatment*, *57*(21), 9982-9992.

Ferkous, H., Merouani, S., & Hamdaoui, O. (2016). Sonolytic degradation of naphthol blue black at 1700 kHz: Effects of salts, complex matrices and persulfate. *Journal of Water Process Engineering*, *9*, 67-77.

Foo, K. Y., & Hameed, B. H. (2012). Preparation, characterization and evaluation of adsorptive properties of orange peel based activated carbon via microwave induced K2CO3 activation. *Bioresource technology*, *104*, 679-686.

Freundlich, H. M. F. (1906). Over the adsorption in solution. *J. Phys. Chem*, *57*(385471), 1100-1107.

Gazi, M., Oladipo, A. A., Ojoro, Z. E. & Gulcan, H. O. 2017 High-performance nanocatalyst for adsorptive and photo-assisted fenton-like degradation of phenol: modeling using artificial neural networks. *Chemical Engineering Communications*, **204**(7), 729-738

Gonçalves, R. G. L., Lopes, P. A., Resende, J. A., Pinto, F. G., Tronto, J., Guerreiro, M. C., ... & Neto, J. L. (2019). Performance of magnetite/layered double hydroxide composite for dye removal via adsorption, Fenton and photo-Fenton processes. *Applied Clay Science*, *179*, 105152.

Gupta, V. K., Ali, I., Saleh, T. A., Nayak, A., & Agarwal, S. (2012). Chemical treatment technologies for waste-water recycling—an overview. *Rsc Advances*, *2*(16), 6380-6388.

Hazzaa, R., & Hussein, M. (2015). Adsorption of cationic dye from aqueous solution onto activated carbon prepared from olive stones. *Environmental Technology & Innovation*, *4*, 36-51.

Ho, Y. S., & McKay, G. (1998). Sorption of dye from aqueous solution by peat. *Chemical engineering journal*, *70*(2), 115-124.

Hu, M., Yan, X., Hu, X., Feng, R., & Zhou, M. (2018). High-capacity adsorption of benzotriazole from aqueous solution by calcined Zn-Al layered double

hydroxides. *Colloids and Surfaces A: Physicochemical and Engineering Aspects*, *540*, 207-214.

Huang, G., Sun, Y., Zhao, C., Zhao, Y., Song, Z., Chen, J., ... & Yin, Z. (2017). Water–n-BuOH solvothermal synthesis of ZnAl–LDHs with different morphologies and its calcined product in efficient dyes removal. *Journal of colloid and interface science*, *494*, 215-222.

Jawad, A., Li, Y., Lu, X., Chen, Z., Liu, W., & Yin, G. (2015). Controlled leaching with prolonged activity for Co–LDH supported catalyst during treatment of organic dyes using bicarbonate activation of hydrogen peroxide. *Journal of hazardous materials*, *289*, 165-173.

Kansal, S. K., Sood, S., Umar, A., & Mehta, S. K. (2013). Photocatalytic degradation of Eriochrome Black T dye using well-crystalline anatase TiO2 nanoparticles. *Journal of Alloys and Compounds*, *581*, 392-397.

Karimi-Shamsabadi, M., Behpour, M., Babaheidari, A. K., & Saberi, Z. (2017). Efficiently enhancing photocatalytic activity of NiO-ZnO doped onto nanozeoliteX by synergistic effects of pn heterojunction, supporting and zeolite nanoparticles in photo-degradation of Eriochrome Black T and Methyl Orange. *Journal of Photochemistry and Photobiology A: Chemistry*, *346*, 133-143.

Kaur, J., & Singhal, S. (2015). Highly robust light driven ZnO catalyst for the degradation of eriochrome black T at room temperature. *Superlattices and Microstructures*, *83*, 9-21.

Kim, S., Durand, P., André, E., & Carteret, C. (2017). Enhanced photocatalytic ability of Cu, Co doped ZnAl based mixed metal oxides derived from layered double hydroxides. *Colloids and Surfaces A: Physicochemical and Engineering Aspects*, *524*, 43-52.

Lagergren, S. K. (1898). About the theory of so-called adsorption of soluble substances. *Sven. Vetenskapsakad. Handingarl*, *24*, 1-39.

Lai, H. T., Hou, J. H., Su, C. I., & Chen, C. L. (2009). Effects of chloramphenicol, florfenicol, and thiamphenicol on growth of algae Chlorella pyrenoidosa, Isochrysis galbana, and Tetraselmis chui. *Ecotoxicology and Environmental safety*, *72*(2), 329-334.

Langmuir, I. (1918). The adsorption of gases on plane surfaces of glass, mica and platinum. *Journal of the American Chemical society*, *40*(9), 1361-1403.

Lee, K. M., Hamid, S. B. A., & Lai, C. W. (2015). Multivariate analysis of photocatalytic-mineralization of Eriochrome Black T dye using ZnO catalyst and UV irradiation. *Materials Science in Semiconductor Processing*, *39*, 40-48.

Lee, S. H., Tanaka, M., Takahashi, Y., & Kim, K. W. (2018). Enhanced adsorption of arsenate and antimonate by calcined Mg/Al layered double hydroxide: Investigation of comparative adsorption mechanism by surface characterization. *Chemosphere*, *211*, 903-911.

Lei, C., Zhu, X., Zhu, B., Jiang, C., Le, Y., & Yu, J. (2017). Superb adsorption capacity of hierarchical calcined Ni/Mg/Al layered double hydroxides for Congo red and Cr (VI) ions. *Journal of hazardous materials*, *321*, 801-811.

Lian, F., Song, Z., Liu, Z., Zhu, L., & Xing, B. (2013). Mechanistic understanding of tetracycline sorption on waste tire powder and its chars as affected by Cu2+ and pH. *Environmental pollution*, *178*, 264-270.

Lin, A. Y. C., Yu, T. H., & Lin, C. F. (2008). Pharmaceutical contamination in residential, industrial, and agricultural waste streams: risk to aqueous environments in Taiwan. *Chemosphere*, *74*(1), 131-141.

Liu, H., Yang, Y., Kang, J., Fan, M., & Qu, J. (2012). Removal of tetracycline from water by Fe-Mn binary oxide. *Journal of Environmental Sciences*, *24*(2), 242-247.

Lu, Y., Jiang, B., Fang, L., Ling, F., Gao, J., Wu, F., & Zhang, X. (2016). High performance NiFe layered double hydroxide for methyl orange dye and Cr (VI) adsorption. *Chemosphere*, *152*, 415-422.

Marzbali, M. H., Esmaieli, M., Abolghasemi, H., & Marzbali, M. H. (2016). Tetracycline adsorption by H3PO4-activated carbon produced from apricot nut shells: A batch study. *Process Safety and Environmental Protection*, *102*, 700-709.

Oladipo, A. A. (2018). MIL-53 (Fe)-based photo-sensitive composite for degradation of organochlorinated herbicide and enhanced reduction of Cr (VI). *Process Safety and Environmental Protection*, *116*, 413-423.

Oladipo, A. A., & Gazi, M. (2014). Enhanced removal of crystal violet by low cost alginate/acid activated bentonite composite beads: optimization and modelling using non-linear regression technique. *Journal of Water Process Engineering*, *2*, 43-52.

Oladipo, A. A., & Ifebajo, A. O. (2018). Highly efficient magnetic chicken bone biochar for removal of tetracycline and fluorescent dye from wastewater: two-stage adsorber analysis. *Journal of environmental management*, *209*, 9-16.

Oladipo, A. A., Abureesh, M. A., & Gazi, M. (2016). Bifunctional composite from spent "Cyprus coffee" for tetracycline removal and phenol degradation: Solar-Fenton process and artificial neural network. *International journal of biological macromolecules*, *90*, 89-99.

Oladipo, A. A., Ifebajo, A. O., Nisar, N., & Ajayi, O. A. (2017). High-performance magnetic chicken bone-based biochar for efficient removal of rhodamine-B

dye and tetracycline: competitive sorption analysis. *Water Science and Technology*, *76*(2), 373-385.

Ou, J., Mei, M., & Xu, X. (2016). Magnetic adsorbent constructed from the loading of amino functionalized Fe3O4 on coordination complex modified polyoxometalates nanoparticle and its tetracycline adsorption removal property study. *Journal of Solid State Chemistry*, *238*, 182-188.

Pouretedal, H. R., Norozi, A., Keshavarz, M. H., & Semnani, A. (2009). Nanoparticles of zinc sulfide doped with manganese, nickel and copper as nanophotocatalyst in the degradation of organic dyes. *Journal of Hazardous Materials*, *162*(2-3), 674-681.

Prasad, C., Tang, H., Liu, Q. Q., Zulfiqar, S., Shah, S., & Bahadur, I. (2019). An overview of semiconductors/layered double hydroxides composites: Properties, synthesis, photocatalytic and photoelectrochemical applications. *Journal of Molecular Liquids*, 111114.

Priya, B., Shandilya, P., Raizada, P., Thakur, P., Singh, N., & Singh, P. (2016). Photocatalytic mineralization and degradation kinetics of ampicillin and oxytetracycline antibiotics using graphene sand composite and chitosan supported BiOCl. *Journal of Molecular Catalysis A: Chemical*, *423*, 400-413.

Raghunath, A., & Perumal, E. (2017). Metal oxide nanoparticles as antimicrobial agents: a promise for the future. *International journal of antimicrobial agents*, *49*(2), 137-152.

Rani, S., Sumanjit, K., & Mahajan, R. K. (2015). Comparative study of surface modified carbonized Eichhornia crassipes for adsorption of dye safranin. *Separation Science and Technology*, *50*(16), 2436-2447.

Rasouli, N., Movahedi, M., & Doudi, M. (2017). Synthesis and characterization of inorganic mixed metal oxide nanoparticles derived from Zn–Al layered double hydroxide and their antibacterial activity. *Surfaces and Interfaces*, *6*, 110-115.

Saratale, R. G., Saratale, G. D., Chang, J. S., & Govindwar, S. P. (2011). Bacterial decolorization and degradation of azo dyes: a review. *Journal of the Taiwan Institute of Chemical Engineers*, *42*(1), 138-157.

Sarmah, A. K., Meyer, M. T., & Boxall, A. B. (2006). A global perspective on the use, sales, exposure pathways, occurrence, fate and effects of veterinary antibiotics (VAs) in the environment. *Chemosphere*, *65*(5), 725-759.

Sayğılı, H., & Güzel, F. (2016). Effective removal of tetracycline from aqueous solution using activated carbon prepared from tomato (Lycopersicon esculentum Mill.) industrial processing waste. *Ecotoxicology and environmental safety*, *131*, 22-29.

Sen, T. K., Afroze, S., & Ang, H. M. (2011). Equilibrium, kinetics and mechanism of removal of methylene blue from aqueous solution by adsorption onto pine cone biomass of Pinus radiata. *Water, Air, & Soil Pollution*, *218*(1-4), 499-515.

Shao, M., Han, J., Wei, M., Evans, D. G., & Duan, X. (2011). The synthesis of hierarchical Zn–Ti layered double hydroxide for efficient visible-light photocatalysis. *Chemical Engineering Journal*, *168*(2), 519-524.

Tang, H., Zhou, W., & Zhang, L. (2012). Adsorption isotherms and kinetics studies of malachite green on chitin hydrogels. *Journal of Hazardous Materials*, *209*, 218-225.

Topal, E. I. A. (2015). Uptake of tetracycline and metabolites in Phragmites australis exposed to treated poultry slaughterhouse wastewaters. *Ecological Engineering*, *83*, 233-238.

Tran, H. N., You, S. J., Hosseini-Bandegharaei, A., & Chao, H. P. (2017). Mistakes and inconsistencies regarding adsorption of contaminants from aqueous solutions: a critical review. *Water research*, *120*, 88-116.

Tu, J., Peng, X., Wang, S., Tian, C., Deng, H., Dang, Z., ... & Lin, Z. (2019). Effective capture of aqueous uranium from saline lake with magnesium-based binary and ternary layered double hydroxides. *Science of The Total Environment*, *677*, 556-563.

United Nations, Department of Economic and Social Affairs, Population Division (2013). World Population Prospects: The 2012 Revision, Highlights and Advance Tables. Working Paper No. ESA/P/WP.228.

Wang, S., & Wu, H. (2006). Environmental-benign utilisation of fly ash as low-cost adsorbents. *Journal of hazardous materials*, *136*(3), 482-501.

Watkinson, A. J., Murby, E. J., Kolpin, D. W., & Costanzo, S. D. (2009). The occurrence of antibiotics in an urban watershed: from wastewater to drinking water. *Science of the total environment*, *407*(8), 2711-2723.

Weber, W. J., & Morris, J. C. (1963). Kinetics of adsorption on carbon from solution. *Journal of the Sanitary Engineering Division*, *89*(2), 31-60.

WHO ref: https://population.un.org/wpp/Publications/Files/WPP2012_HIGHLIGHTS.pdf

World Health Organization (WHO), Health and Environment in Sustainable Development: Five Years After the Earth Summit, WHO Geneva, 1997.

World Population Review. Accessed online on August 10, 2019 from http://worldpopulationreview.com/world-cities/cape-town-population/

Xia, S. J., Liu, F. X., Ni, Z. M., Xue, J. L., & Qian, P. P. (2013). Layered double hydroxides as efficient photocatalysts for visible-light degradation of Rhodamine B. *Journal of colloid and interface science*, *405*, 195-200.

Yang, X., Xu, G., Yu, H., & Zhang, Z. (2016). Preparation of ferric-activated sludge-based adsorbent from biological sludge for tetracycline removal. *Bioresource technology*, *211*, 566-573.

Yao, W., Yu, S., Wang, J., Zou, Y., Lu, S., Ai, Y., ... & Wang, X. (2017). Enhanced removal of methyl orange on calcined glycerol-modified nanocrystallined Mg/Al layered double hydroxides. *Chemical Engineering Journal*, *307*, 476-486.

Yu, F., Li, Y., Han, S., & Ma, J. (2016). Adsorptive removal of antibiotics from aqueous solution using carbon materials. *Chemosphere*, *153*, 365-385.

Zubair, M., Daud, M., McKay, G., Shehzad, F., & Al-Harthi, M. A. (2017a). Recent progress in layered double hydroxides (LDH)-containing hybrids as adsorbents for water remediation. *Applied Clay Science*, *143*, 279-292.

Zubair, M., Jarrah, N., Manzar, M. S., Al-Harthi, M., Daud, M., Mu'azu, N. D., & Haladu, S. A. (2017b). Adsorption of eriochrome black T from aqueous phase on MgAl-, CoAl-and NiFe-calcined layered double hydroxides: Kinetic, equilibrium and thermodynamic studies. *Journal of molecular liquids*, *230*, 344-352.